Supporting Information

Evidence for a boride–borylene-ligand-tautomerism leading to a remote C–C-bond and concomitant boryl ligand formation

Frerk-Ulfert Wehmeyer,[a] Yinwu Li,[b] Anne Schlossarek,[a] Zhuofeng Ke[b] and Robert Langer[a,*]

[a] Institute of Chemistry, Faculty of Natural Sciences II, Martin-Luther-Universität Halle- Wittenberg, Kurt-Mothes- Str. 2, D-06120 Halle (Saale), Germany. Fax: +49 (0)345 5527028; Tel: +49 (0)345 5525620; E-mail: robert.langer@chemie.uni-halle.de

[b] School of Materials Science Engineering, PCFM Lab, Sun Yat-sen University, Guangzhou 510275, China

Contents

Materials and Methods

All experiments were carried out under an atmosphere of purified argon 5.0 in the MBraun LABmaster and GS MEGA glove box or using standard Schlenk techniques.

Diethylether and tetrahydrofuran were dried with Sodium. *n*-Hexane was dried with Lithium aluminium hydride. Dichloromethane was dried with lithium hydride. After drying, solvents were stored over appropriate molecular sieves.

Deuterated solvents were degassed with freeze-pump-thaw cycles and stored over appropriate molecular sieves under argon atmosphere. ^{1}H, ^{13}C, ^{11}B, ^{19}F and ^{31}P NMR spectra were recorded using Agilent Technologies 400 MHz VNMRS and 500 MHz DD2 NMR spectrometers at 300 K. ^{1}H and $^{13}C\{^{1}H\}$, ^{13}C-APT (attached proton test) NMR chemical shifts are reported in ppm referenced to tetramethylsilane. The resonance of the residual protons in the deuterated solvent was used as internal reference for ^{1}H NMR spectra. The solvent peak of the deuterated solvent was used as internal reference for ^{13}C APT NMR spectra. ^{11}B NMR chemical shifts are reported in ppm referenced to $BF_3(OEt_2)$ as external standard. ^{19}F NMR chemical shifts are reported in ppm with respect to $CFCl_3$ and referenced to liquid $CFCl_3$ as external standard. ^{31}P NMR chemical shifts are reported in ppm with respect to H_3PO_4 and referenced to an external 85 % solution of phosphoric acid in D_2O. The following abbreviations are used for the description of NMR data: br (broad), s (singlet), d (doublet), t (triplet), q (quartet), quin (quintet), m (multiplet).

FT-IR spectra were recorded by attenuated total reflection (ATR) of the solid samples on a Bruker Tensor 27 spectrometer at ambient temperature. The intensity of the absorption band is indicated as w (weak), m (medium), s (strong), vs (very strong) and br (broad).

High-resolution mass spectra were recorded on a Thermo Scientific Q Exactive Plus spectrometer equipped with an Orbitrap Mass Analyzer and Thermo Scientific HESI-II (heated electro spray ionization). External mass calibration was performed in HESI mode by measuring calmix provided from Thermo Scientific. LTQ Velos ESI Positiv Ion Calibration Solution and ESI Negativ Ion Calibration Solution, respectively.

Elemental analyses by combustion analysis were performed in a Unicube (Elementar) using argon as carrier/shielding gas and tin foil crucibles for sample preparation, as well as in an Elementar-Vario EL using helium as carrier/shielding gas.

UV-Vis experiments were conducted with the UV-Vis spectrometer Agilent Technologies Cary 60. For the temperature dependent measurements, a Hellma Analytics Transition Probe Excalibur was connected with the spectrometer.

Cyclic voltammetry measurements were performed with a Metrohm µStat 400. After each experiment ferrocene was added for a calibration experiment and the potentials were referenced against the ferrocene/ferrocenium redox couple.

Synthesis of $[H_2B(PPh_2Py\text{-}\kappa N)_2](PF_6)$ (1)

Diphenyl-2-pyridylphosphane (5000 mg, 19.0 mmol) and KPF_6 (10486 mg, 57.0 mmol) were dissolved in 200 mL CH_2Cl_2 and a solution of $BH_2Br{\cdot}SMe_2$ in CH_2Cl_2 (1 M, 9.5 mL, 9.5 mmol) was added. The solution was stirred for 6 d and layered with *n*-hexane, which resulted in yellow crystals. Yield: 5513 mg (8.06 mmol, 84.8 %). Anal. Calcd for $C_{34}H_{30}BF_6N_2P_3$: C, 59.67; H, 4.42; N, 4.09. Found: C, 59.38; H,

4.31; N, 3.97. ^{1}H NMR (499.72 MHz, CD_2Cl_2, 27 °C) δ = 7.25 - 7.19 (m, 8H, H_{Ph}), 7.29 (dd, 2H, $^{3}J_{HH}$ = 8.0, $^{4}J_{HP}$ 1.5 Hz, 3-H_{Py}), 7.44 - 7.39 (m, 8H, H_{Ph}), 7.49 - 7.44 (m, 4H, H_{Ph}), 7.69 (ddd, 2H, $^{3}J_{HH}$ = 7.6, $^{3}J_{HH}$ = 5.9, $^{4}J_{HP}$ = 1.5 Hz, 5-H_{Py}), 8.00 (td, 2H, $^{3}J_{HH}$ = 7.9, $^{5}J_{HP}$ = 1.6 Hz, 4-H_{Py}), 8.43 (d, 2H, $^{3}J_{HH}$ = 5.9 Hz, 6-H_{Py}) ppm. Only resonances that are changing upon decoupling are listed for the 1H{11B} NMR spectrum. ^{1}H{^{11}B} NMR (499.72 MHz, CD_2Cl_2, 27 °C) δ/ppm = 4.04 (s, 2H, BH_2) ppm. ^{13}C APT NMR (126 MHz, CD_2Cl_2, 27 °C) δ = 127.0 (s, 3-C_{Ph}), 129.8 (m, C_{Ph}), 130.9 (s, C_{Ph}), 133.0 (m, C_{Ph}), 133.4 (s, C_{Py}), 134.9 (m, 6-C_{Ph}), 150.4 (s, C_{Py}), 142.8 (s, C_{Py}), 164.2 (d, $^{1}J_{CP}$ = 27.5 Hz, 2-C_{Py}) ppm. ^{31}P{^{1}H} NMR (202 MHz, CD_2Cl_2, 27 °C) δ = -144.6 (hept, $^{1}J_{PF}$ = 711.0 Hz), -7.3 (s) ppm. ^{19}F{^{1}H} NMR (470 MHz, CD_2Cl_2, 27 °C) δ = -73.1 (d, $^{1}J_{FP}$ = 710.9 Hz) ppm. ^{11}B{^{1}H} NMR (139 MHz, CD_2Cl_2, 27 °C) δ = -1.9 ppm. FT-IR (ATR) ũ / cm-1: 2464 (w), 2445 (w), 1600 (w), 1565 (w), 1469 (w), 1434 (w), 1317 (w), 1292 (w), 1243 (w), 1197 (w), 1183 (w), 1158 (w), 1127 (w), 1108 (w), 1091 (w), 1081 (w), 1053 (w), 1025 (w), 999 (w), 879 (w), 834 (s), 787 (m), 756 (m), 745 (m), 697 (m), 619 (w), 601 (w), 558 (m), 499 (m).

Synthesis of [(HB{PPh_2Py}$_2$)Rh(CO)$_2$]PF_6 (2)

$Rh_2(CO)_4Cl_2$ (112.8 mg, 0.290 mmol), [$H_2B(PPh_2Py$-κ*N*)$_2$](PF_6) (**1**, 397.0 mg, 0.580 mmol) and DABCO (200 mg, 1.76 mmol) were dissolved in 20 mL THF and stirred for 3 h. The product was precipitated by 200 mL of a mixture of Hexane/Et_2O 1:1 (v/v) and dried in vacuo. Yield: 450.1 mg (0.534 mmol, 92.1 %). Anal. Calcd for $C_{36}H_{29}BF_6N_2O_2P_3Rh$: C, 51.34; H, 3.47; N, 3.33. Found: C, 50.94; H, 3.52; N, 3.03. ^{1}H NMR (499.72 MHz, CD_2Cl_2, 27 °C) δ = 7.01 (m, 4H, H_{Ph}), 7.26 (t, 4H, J = 7.5 H_{Ph}), 7.35 (t, 2H, J = 7.4 Hz, H_{Ph}), 7.44 (d, 2H, J = 7.8 Hz, 3-H_{Py}), 7.56-7.46 (m, 6H, H_{Ph}), 7.66 (m, 4H, H_{Ph}), 7.71 (t, 2H, J = 6.7 Hz, 5-H_{Py}), 7.95 (t, 2H, J = 7.7 Hz, 4-H_{Py}), 8.45 (d, 2H, J = 5.7 Hz, 6-H_{Py}) ppm. Only resonances that are changing upon decoupling are listed for the ^{1}H{^{11}B} NMR spectrum. ^{1}H{^{11}B} NMR (499.72 MHz, CD_2Cl_2, 27 °C) δ = 5.11 (br) ppm. ^{13}C APT NMR (126 MHz, CD_2Cl_2, 27 °C) δ = 127.9 (s, 5-C_{Py}), 129.5 (t, J = 4.9 Hz, C_{Ph}), 129.6 (t, J = 5.5 Hz, C_{Ph}), 130.6 (s, 3-C_{Py}), 130.7 (s, C_{Ph}), 131.7 (s, C_{Ph}), 132.1 (t, J = 7.3, C_{Ph}), 133.9 (d, J = 21.3 Hz, 1-C_{Ph}), 134.2 (t, J = 9.4, C_{Ph}), 134.8 (t, J = 16.2 Hz, 1-C_{Py}), 142.5 (s, 4-C_{Py}), 147.5 (t, J = 6.2, 6-C_{Py}), 163.7 (t, J = 19.4 Hz, 2-C_{Py}) ppm. ^{31}P{^{1}H} NMR (202 MHz, CD_2Cl_2, 27 °C) δ = -144.6 (hept, $^{1}J_{PF}$ = 711.1 Hz), 49.9 Hz (d, $^{1}J_{PRh}$ =163.8 Hz) ppm. ^{19}F{^{1}H} NMR (470 MHz, CD_2Cl_2, 27 °C) δ = -72.8 Hz (d, $^{1}J_{FP}$ = 711.1) ppm. ^{11}B{^{1}H} NMR (139 MHz, CD_2Cl_2, 27 °C) δ = 17.0 (br) ppm. FT-IR (ATR) ũ / cm-1: 3057 (w), 2431 (w), 2362 (w), 2334 (w), 2018 (m), 1956 (s), 1916 (w), 1598 (w), 1471 (w), 1436 (w), 1335 (w), 1311 (w), 1286 (w), 1263 (w) 1184 (w), 1087 (w), 1066 (w), 1039 (w) 997 (w), 919 (w), 880 (w), 836 (s), 775 (w), 760 (w), 746 (m), 728 (w), 695 (m), 630 (w), 607 (w), 574 (m), 559 (m), 535 (w), 517 (m), 509 (m), 501 (m), 472 (m), 436 (m), 422 (m), 411 (m), 395 (w), 383 (w). HR-HESI-MS (pos. mode) m/z: 669.08977 (calculated for [(HB{PPh_2Py}$_2$)Rh(CO)]$^{+}$), 669.0898 (found, Δ = 0.03 ppm).

Synthesis of [(HB{Hbipy})Rh(CO)$_2$]PF_6 (3)

[(HB{PPh_2Py}$_2$)Rh(CO)$_2$]PF_6 (**2**, 50.0 mg, 0.059 mmol) was dissolved in 2 mL THF. A solution of LiHMDS (11.4 mg, 0.063 mmol) in 2 mL THF was added dropwise at -90 °C. The solution was allowed to warm to RT and layered with n-hexane to obtain red crystals after three days. Yield: 24.8 mg (0.036 mmol, 60.0 %). Anal. Calcd for $C_{36}H_{28}BN_2O_2P_2Rh$: C, 62.10; H, 4.05; N, 4.02. Found: C, 61.61; H, 4.10; N, 3.87. ^{1}H NMR (499.72 MHz, CD_2Cl_2, 27 °C) δ = 4.69 (t, 1H, 5.4 Hz, 3-H_{HPy}) ppm, 5.22 (d, 1H, 5.8 Hz, 6-H_{HPy}), 5.62 (m, 1H, 5-H_{Py}), 6.14 (ddd, 1H, J = 9.3, 5.6, 2.0 Hz, 4-H_{Py}), 6.96 (m, 2H, H_{Ph}), 7.10 (m, 2H, H_{Ph}), 7.21 (m, 3H, H_{Ph}), 7.31 (m, 2H, H_{Ph}), 7.35 (dd, 1H, J = 7.7, 2.9 Hz, 3-H_{Py}), 7.40 (ddd, 2H, J = 16.3, 7.3, 1.5 Hz), 7.43-7.50 (m, 5H, H_{Ph}), 7.51 (s, 1H, 5-H_{Py}), 7.82 (t, 1H, J = 7.6 Hz, 4-H_{Py}), 7.88 (m, 4H, H_{Ph}) ppm. Only resonances that are changing upon decoupling are listed for the ^{1}H{^{11}B} NMR spectrum. ^{1}H{^{11}B} NMR (499.72 MHz, CD_2Cl_2, 27 °C) δ = 4.58 ppm ^{13}C APT NMR (126 MHz, CD_2Cl_2, 27 °C) δ = 61.6 (d, J = 15.4 Hz, 6-C_{HPy}), 103.4 (d, J = 5.4 Hz, 3-C_{HPy}), 109.3 (d, J = 2.1 Hz, 5-C_{HPy}), 119.9 (s, 3-C_{Py}), 125.6 (s, 5-C_{Py}),

127.5 (d, J = 9.3 Hz, C_{Ph}), 128.1 (d, J = 9.6 Hz, C_{Ph}), 128.2 (d, J = 5.5 Hz, 4-C_{HPy}), 128.4 (d, J = 8.8 Hz, C_{Ph}), 128.5 (d, J = 9.6 Hz, C_{Ph}), 128.6 (d, J = 1.6 Hz, C_{Ph}), 129.0 (d, J = 1.6 Hz, C_{Ph}), 129,5 (d, J = 1.2 Hz, C_{Ph}), 129.8 (d, J = 1.5 Hz, C_{Ph}), 132.0 (d, J = 14.5 Hz, C_{Ph}), 132.3 (dd, J = 13.8, 2.4 Hz, C_{Ph}), 132,8 (dd, J = 14.7, 3.1 Hz, C_{Ph}), 137.1 (m, C_{Ph}), 138,2 (d, J = 28.2 Hz, C_{Ph}), 139.2 (s, 4-C_{Py}), 139.6 (dd, J = 34.1, 13.2 Hz, C_{Ph}), 154.8 (d, J = 50.8 Hz, 2-C_{HPy}), 156.0 (d, J = 32.9 Hz, 6-C_{Py}), 163.1 (d, J = 13.4 Hz, 1-C_{Py}) ppm. $^{31}P\{^{1}H\}$ NMR (202 MHz, CD_2Cl_2, 27 °C) δ = 60.1 (m) ppm. $^{11}B\{^{1}H\}$ NMR (160 MHz, CD_2Cl_2, 27 °C) δ = 13.3 (br) ppm. FT-IR (ATR) ũ / cm-1: 3047 (w), 2358 (w), 1986 (m), 1965 (w), 1934 (s), 1900 (w), 1620 (w) 1587 (w), 1525 (w), 1480 (w), 1456 (w), 1434 (m), 1402 (w), 1356 (w), 1306 (w), 1289 (w), 1253 (w), 1182 (w), 1156 (w), 1142 (w), 1123 (w), 1091 (w), 1072 (w), 1051 (w), 1027 (m), 1007 (m), 943 (w), 911 (w), 874 (w), 844 (w), 807 (w), 793 (w), 781 (w), 744 (m), 721 (w), 695 (s), 636 (w), 622 (w), 595 (w), 577 (w), 559 (w), 547 (w), 536 (w), 514 (s), 497 (m), 480 (m), 468 (m), 457 (m), 423 (m), 408 (m), 373 (m). LIFDI-MS (pos. mode) m/z: 638.08977 (calculated for $[(HB\{PPh_2Py\}_2)Rh(CO)(-H)]^+$), 669.0904 (found, Δ = 0.98 ppm).

Electrochemistry data

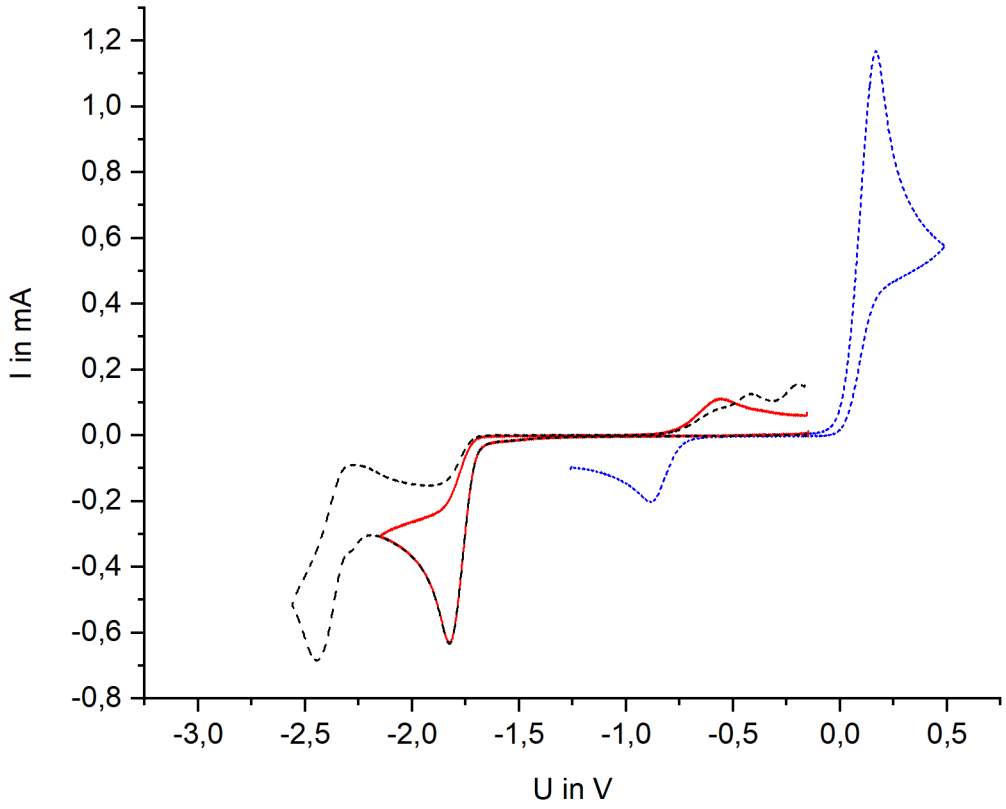

Figure 1 Cyclic voltammograms of **2** in a solution of tetrabutylammonium phosphate (0.1 mol/L) in tetrahydrofuran. Peaks potentials are actuated separately to show dependent return wave processes. The voltammograms shows an oxidation peak at +0.16 V (blue dotted) and reduction peaks at -1.83 V (red) and -2.43 V (black dashed) vs. Fc/Fc^{+}. All processes are non-reversible.

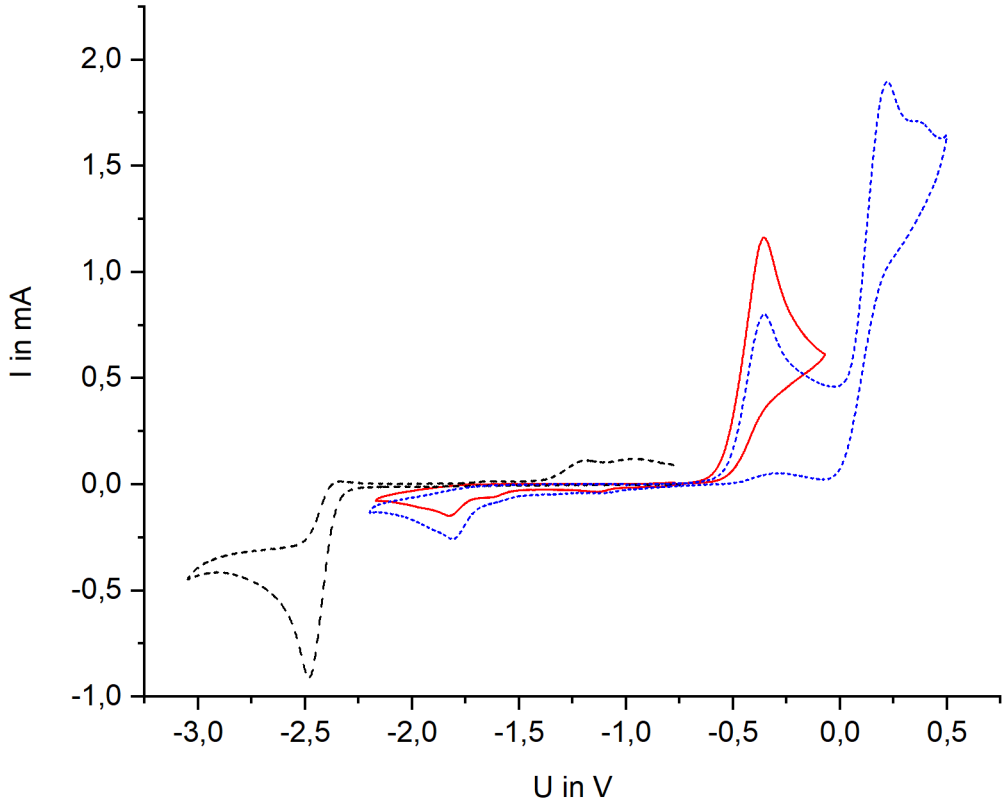

Figure 2 Cyclic voltammograms of **3** in a solution of tetrabutylammonium phosphate (0.1 mol/L) in tetrahydrofuran. Peaks potentials are actuated separately to show dependent return wave processes. The voltammograms shows an oxidation peak at +0.21 V (blue dotted) and reduction peaks at -0.36 V (red) and -2.48 V (black dashed) vs. Fc/Fc^{+}. All processes are non-reversible.

UV-Vis spectra

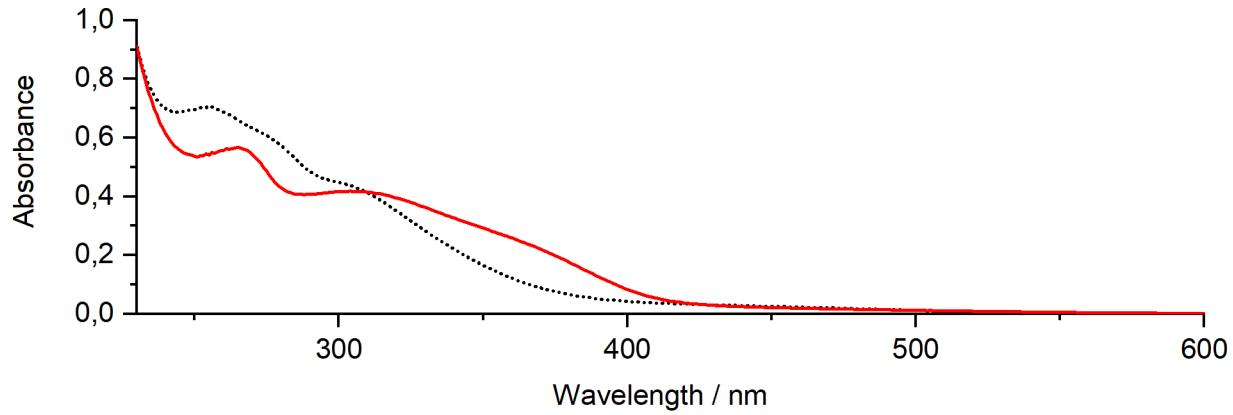

Figure 3 UV-Vis spectra of **2** (black dotted) and **3** (red), concentration 2,38 · 10^{-5} mol/L

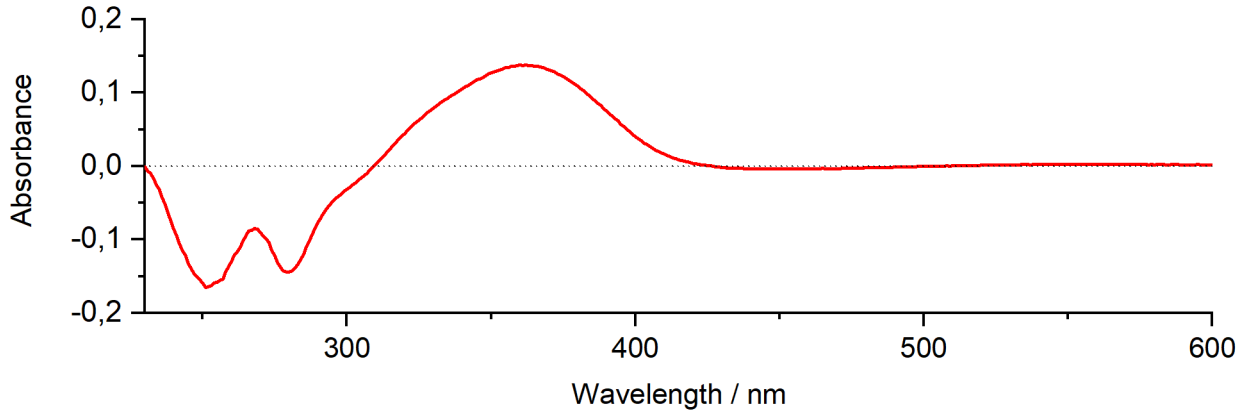

Figure 4 Difference between the UV-Vis spectra of **2** and **3**, concentration 2,38 · 10^{-5} mol/L

UV/Vis spectroscopic monitoring of the Reaction of 2 with $LiN(SiMe_3)_2$

The reaction was performed analogous to the preparation of **3**, but in a higher dilution and, to compensate this, with 3 eq $LiN(SiMe_3)_2$. Complex **2** (15.0 mg, 0.018 mmol) was dissolved in 145 mL THF. At -40 °C a solution of $LiN(SiMe_3)_2$ (8.7 mg, 0.052 mmol) in 2 mL THF was added. While the solution was allowed to slowly warm up, UV-Vis spectra were measured with a submersible probe every five minutes. The temperature was calculated with a polynomial fit, so the absorbance can be examined as function of the temperature.

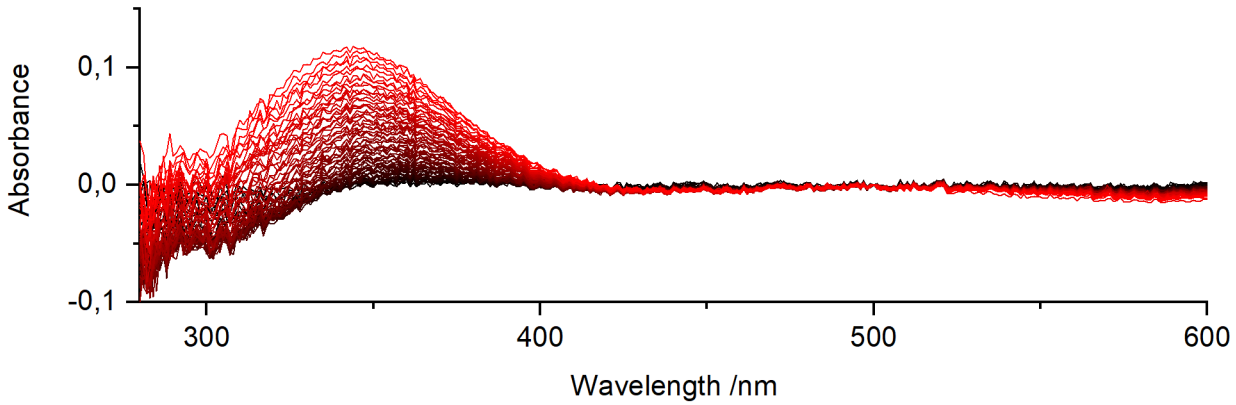

Figure 5 shift of the UV-Vis spectra of the reaction of **2** with 3 eq $LiN(SiMe_3)_2$, measured in intervals of 5 min (t = 0, black; t= 345 min, red)

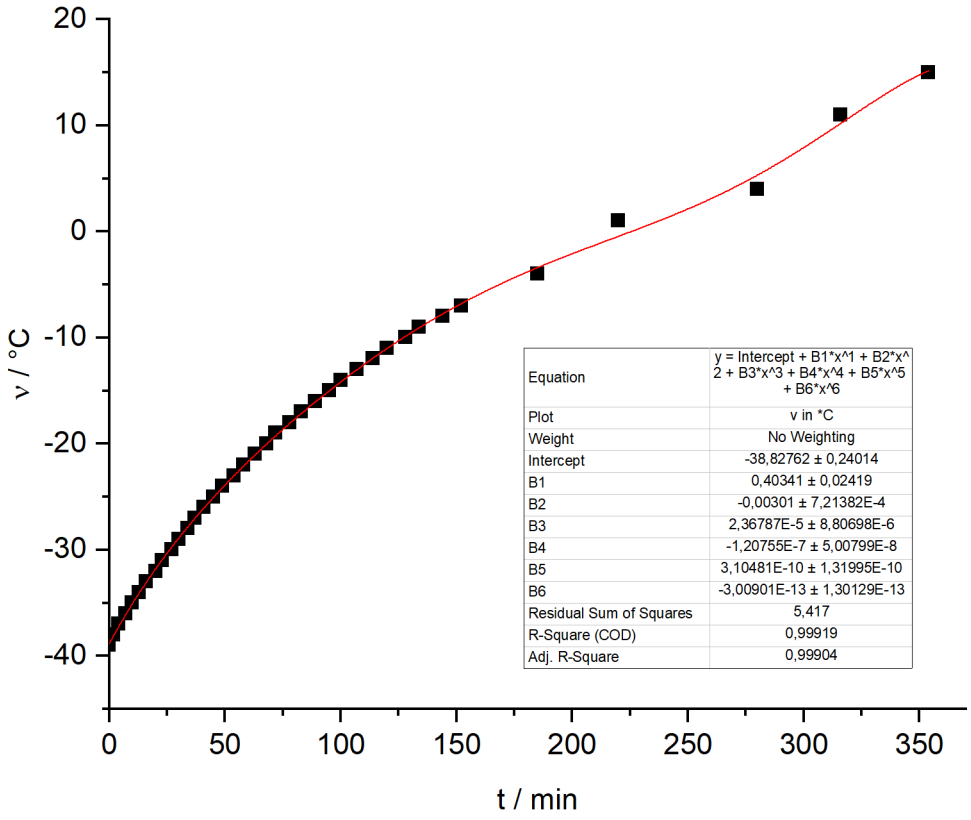

Figure 6 Measured temperature in dependence to the time. A polynomial fit was calculated with Origin.

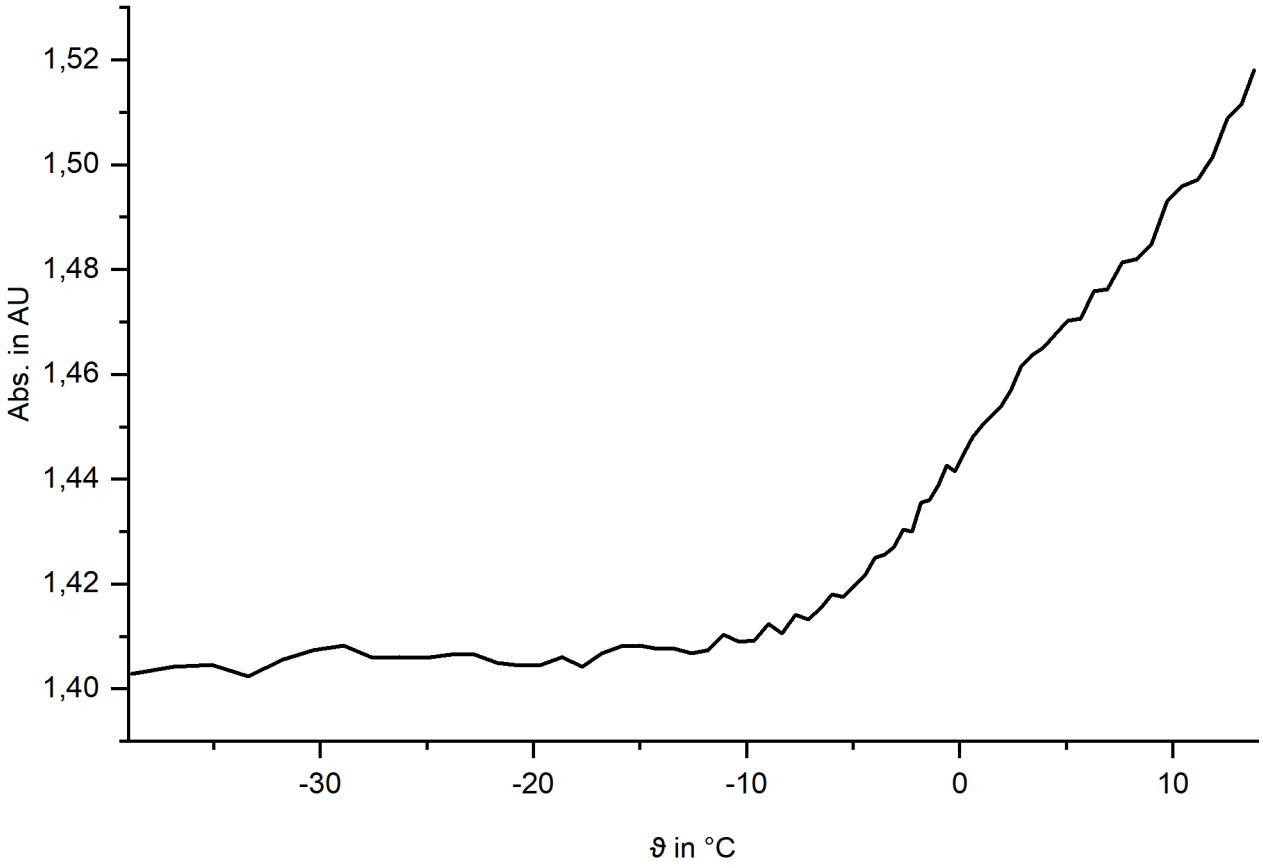

Figure 7 Change of the absorbance at 344 nm in dependence of the temperature

NMR Spectra

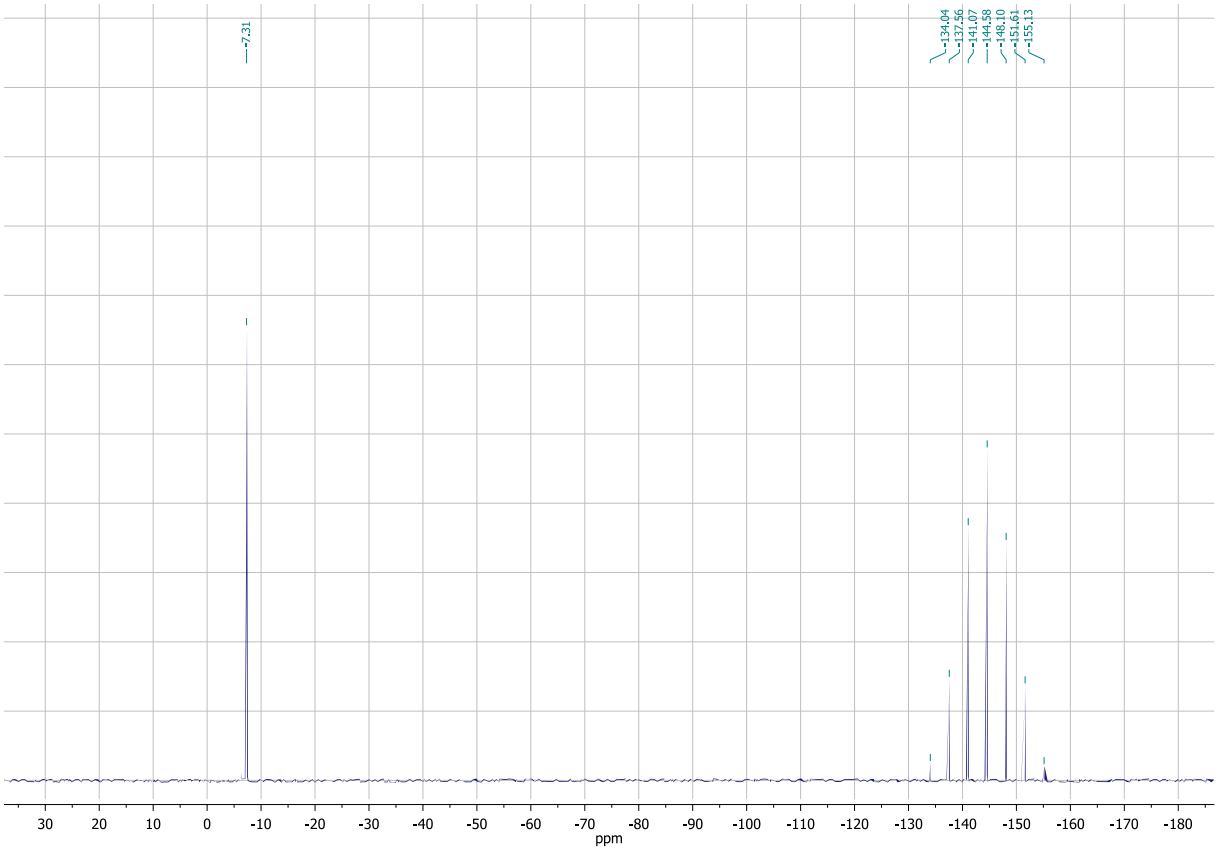

Figure 8 $^{31}P\{^{1}H\}$ NMR (202 MHz, CD_2Cl_2) spectrum of **1**

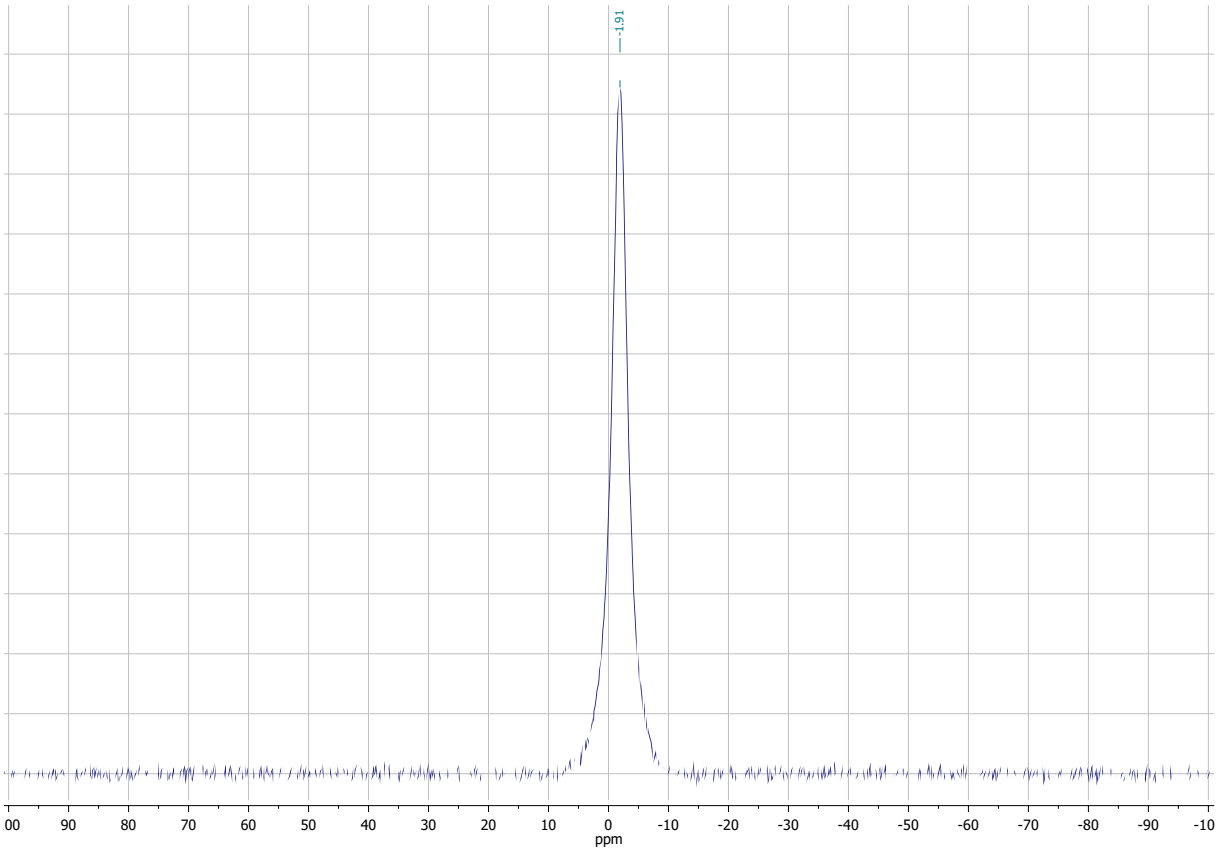

Figure 9 $^{11}B\{^{1}H\}$ NMR (129 MHz, CD_2Cl_2, 27 °C) spectrum of 1

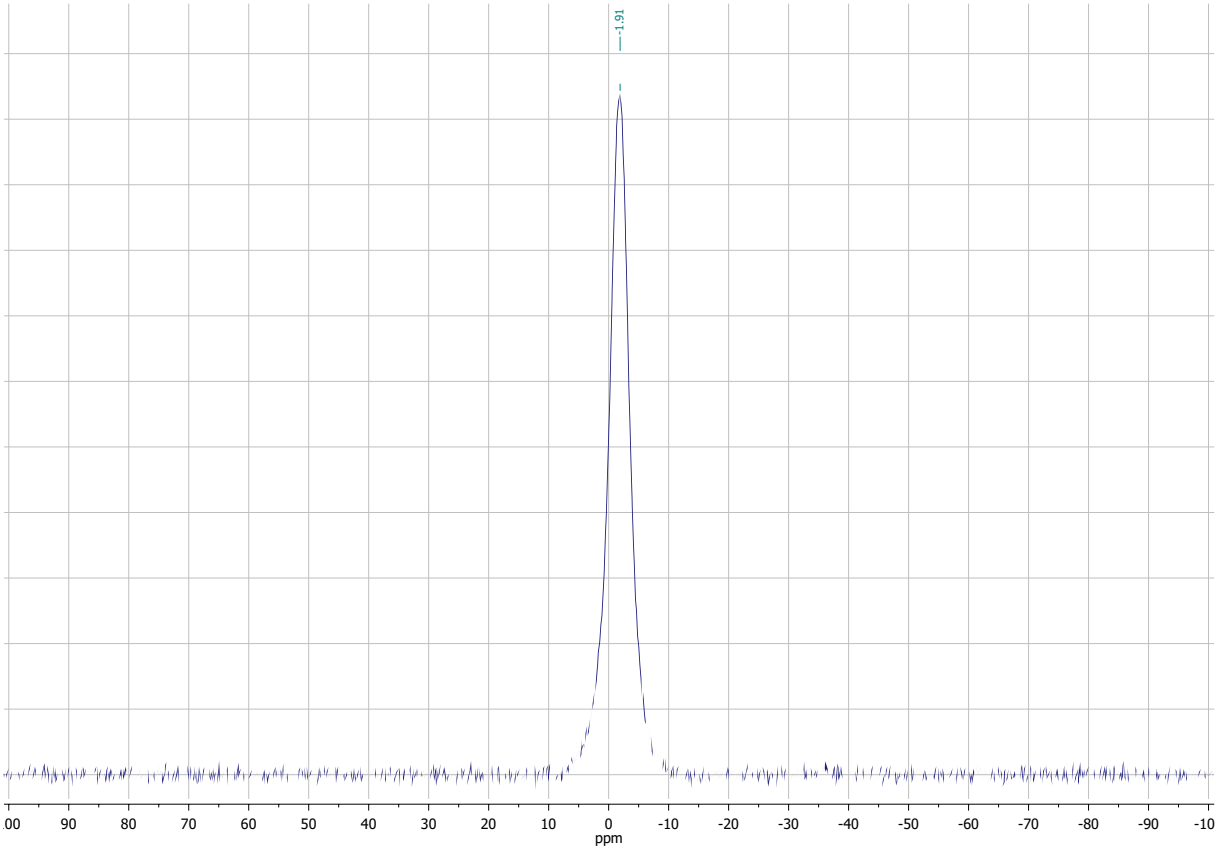

Figure 10 ^{11}B NMR (129 MHz, CD_2Cl_2, 27 °C) spectrum of **1**

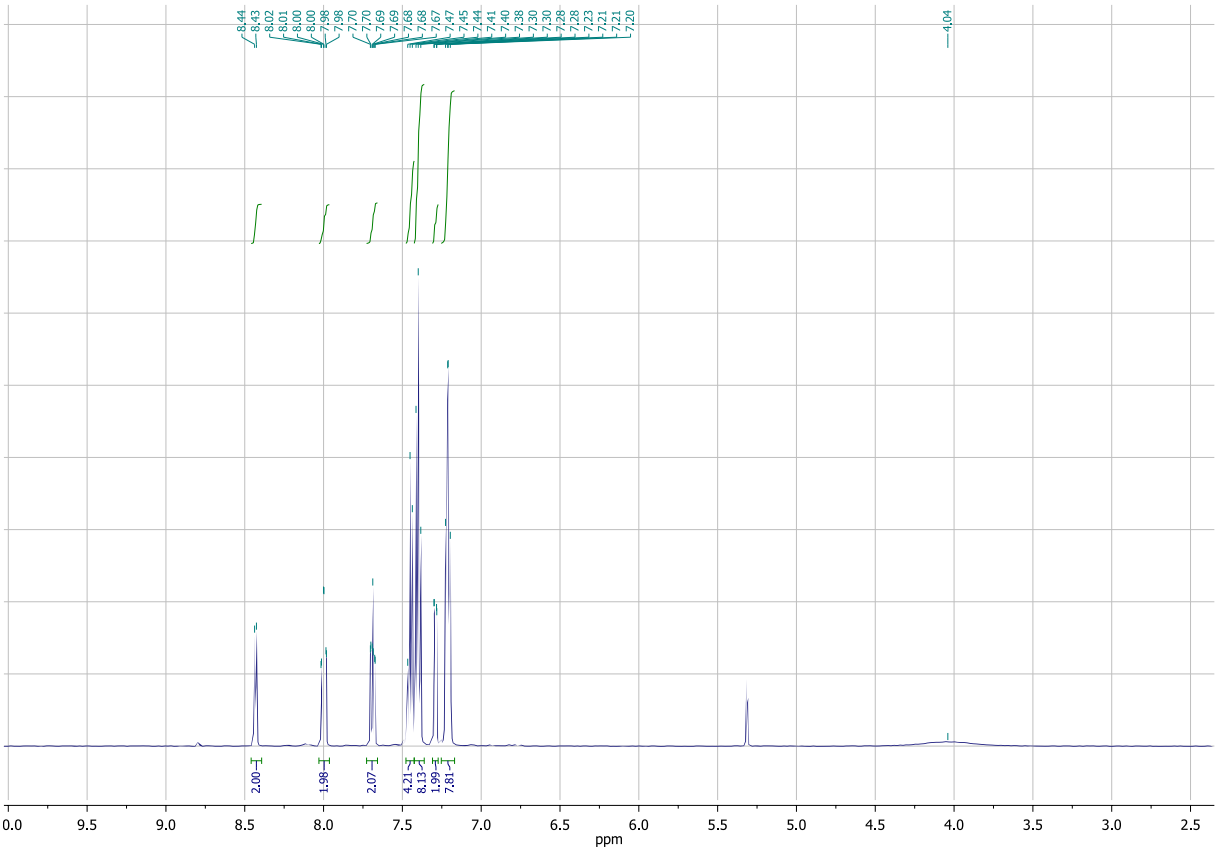

Figure 11 ^{1}H NMR (499.72 MHz, CD_2Cl_2, 27 °C) spectrum of **1**

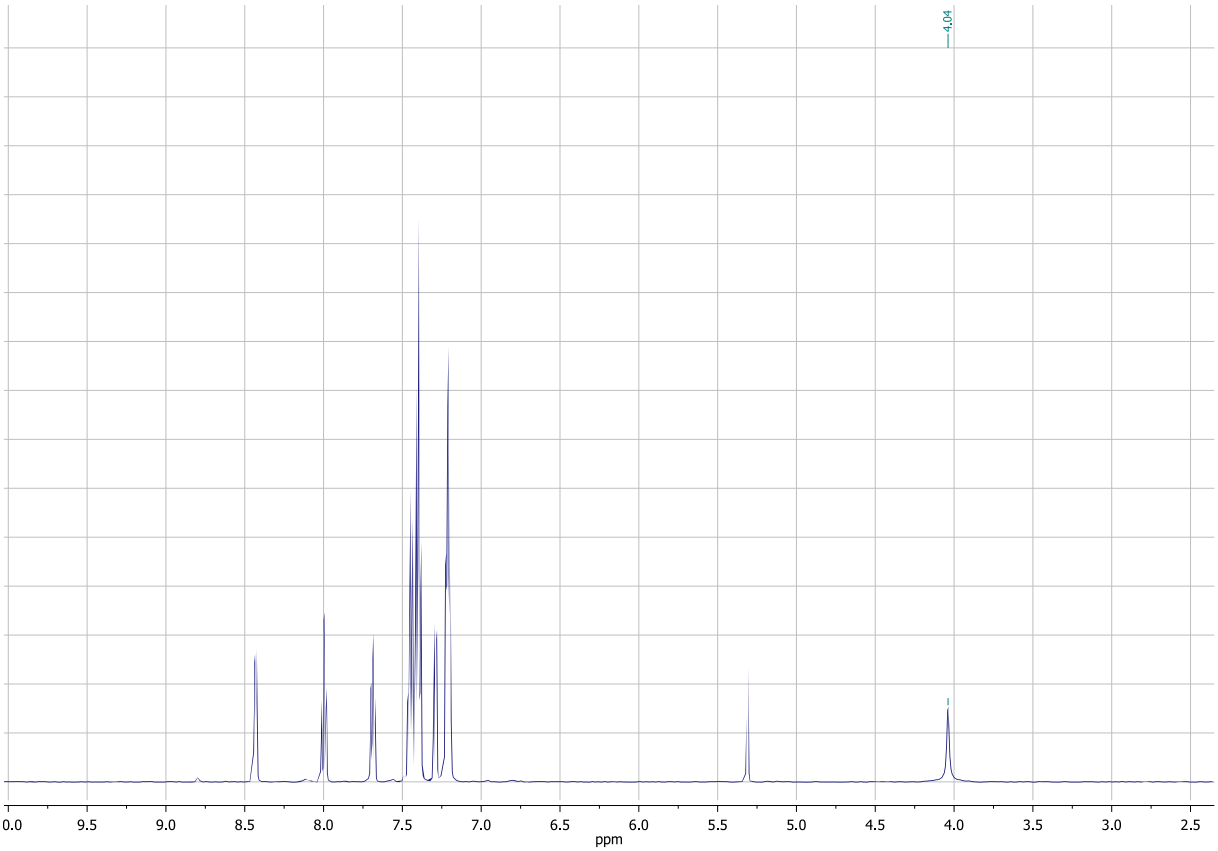

Figure 12 $^{1}H\{^{11}B\}$ NMR (499.72 MHz, CD_2Cl_2, 27 °C) spectrum of **1**

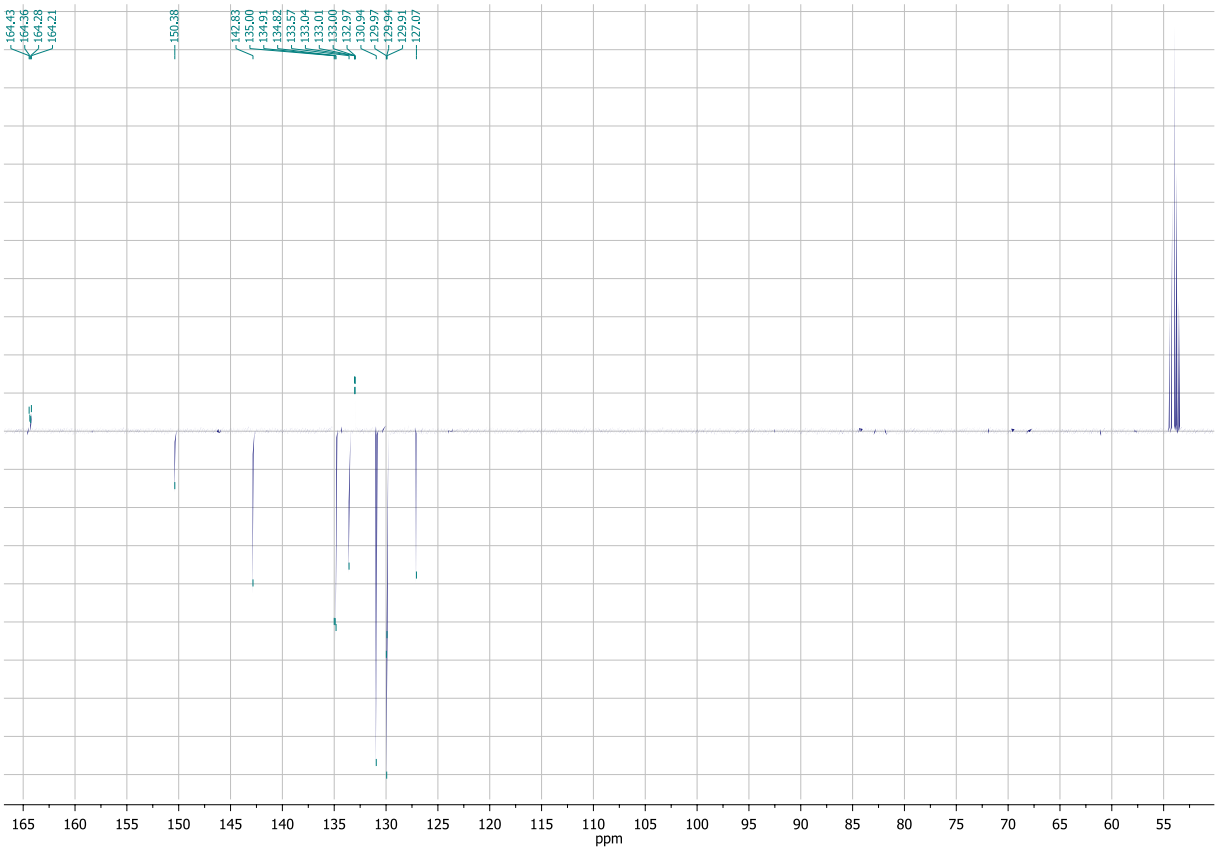

Figure 13 ^{13}C APT NMR (126 MHz, CD_2Cl_2, 27 °C) spectrum of **1**

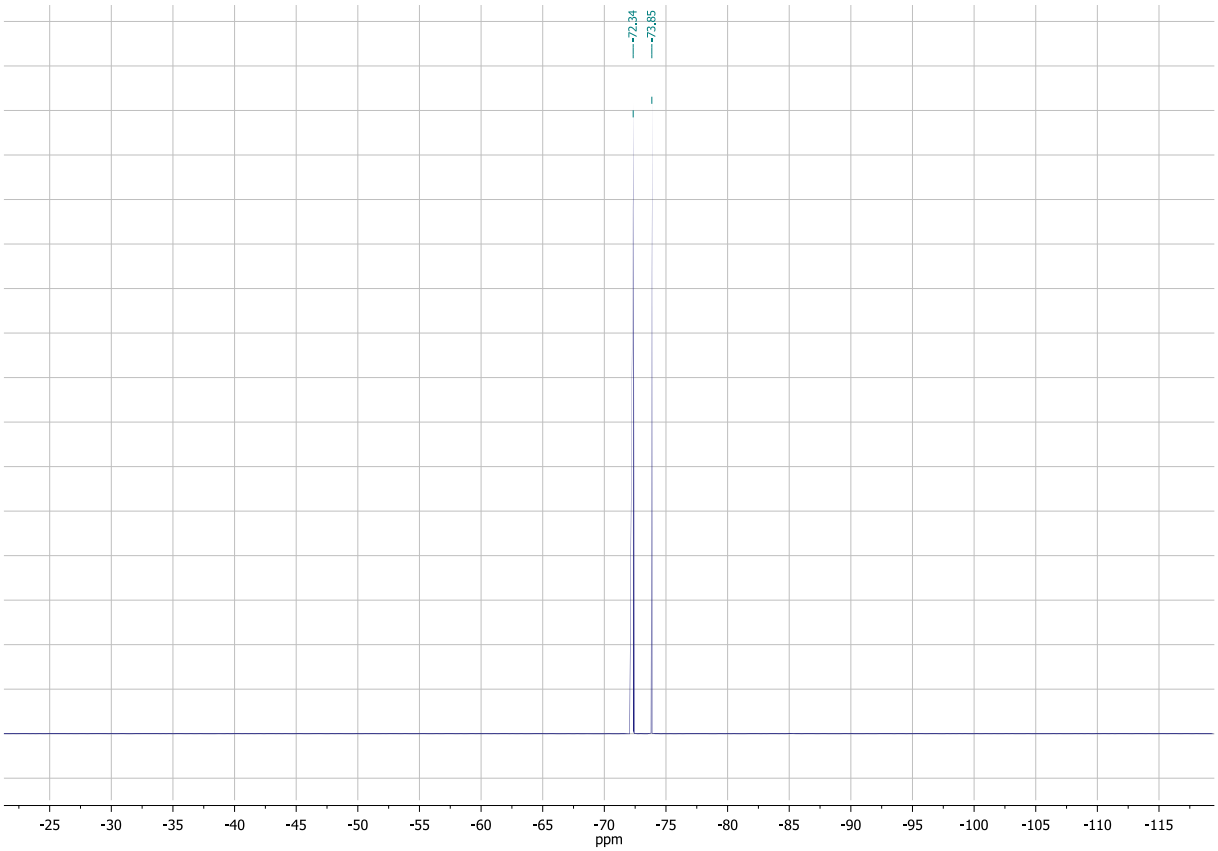

Figure 14 $^{19}F\{^{1}H\}$ NMR (470 MHz, CD_2Cl_2, 27 °C) spectrum of **1**

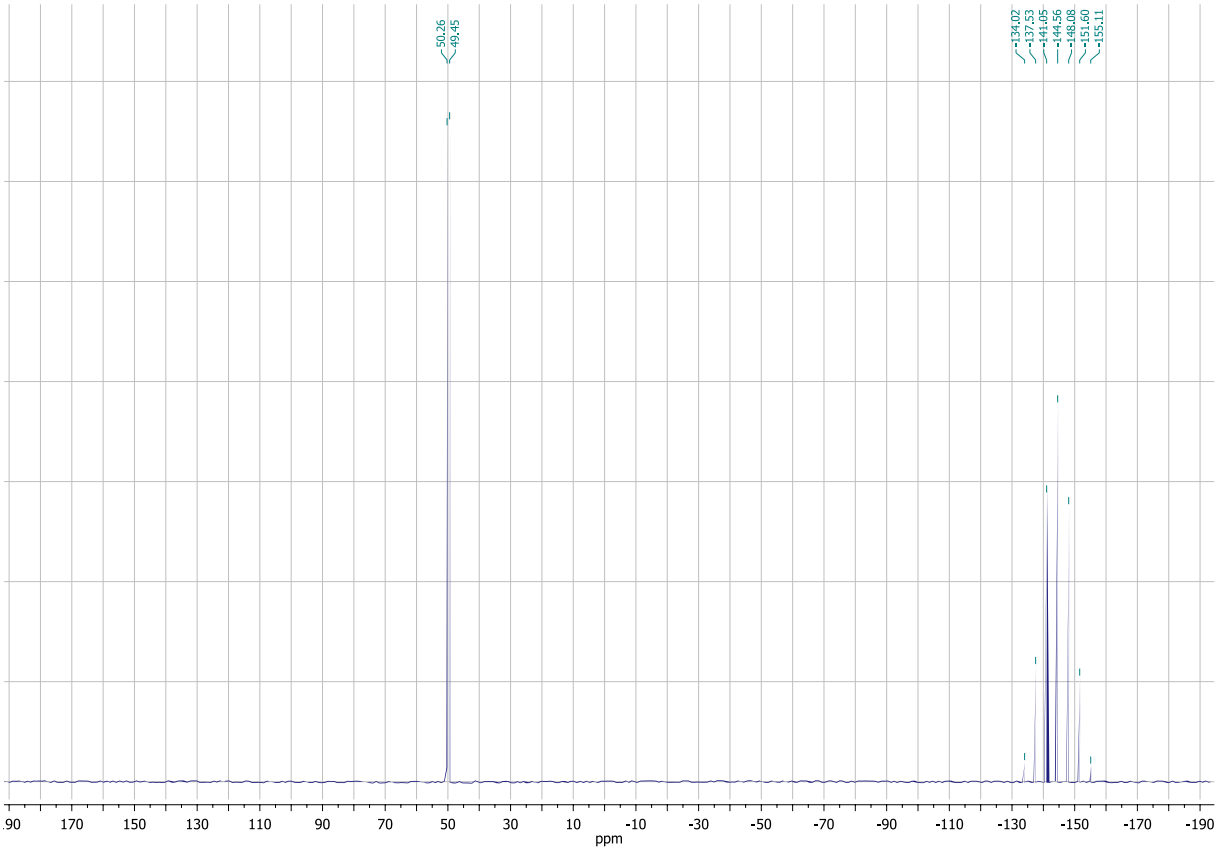

Figure 15 $^{31}P\{^{1}H\}$ NMR (202 MHz, CD_2Cl_2) spectrum of **2**

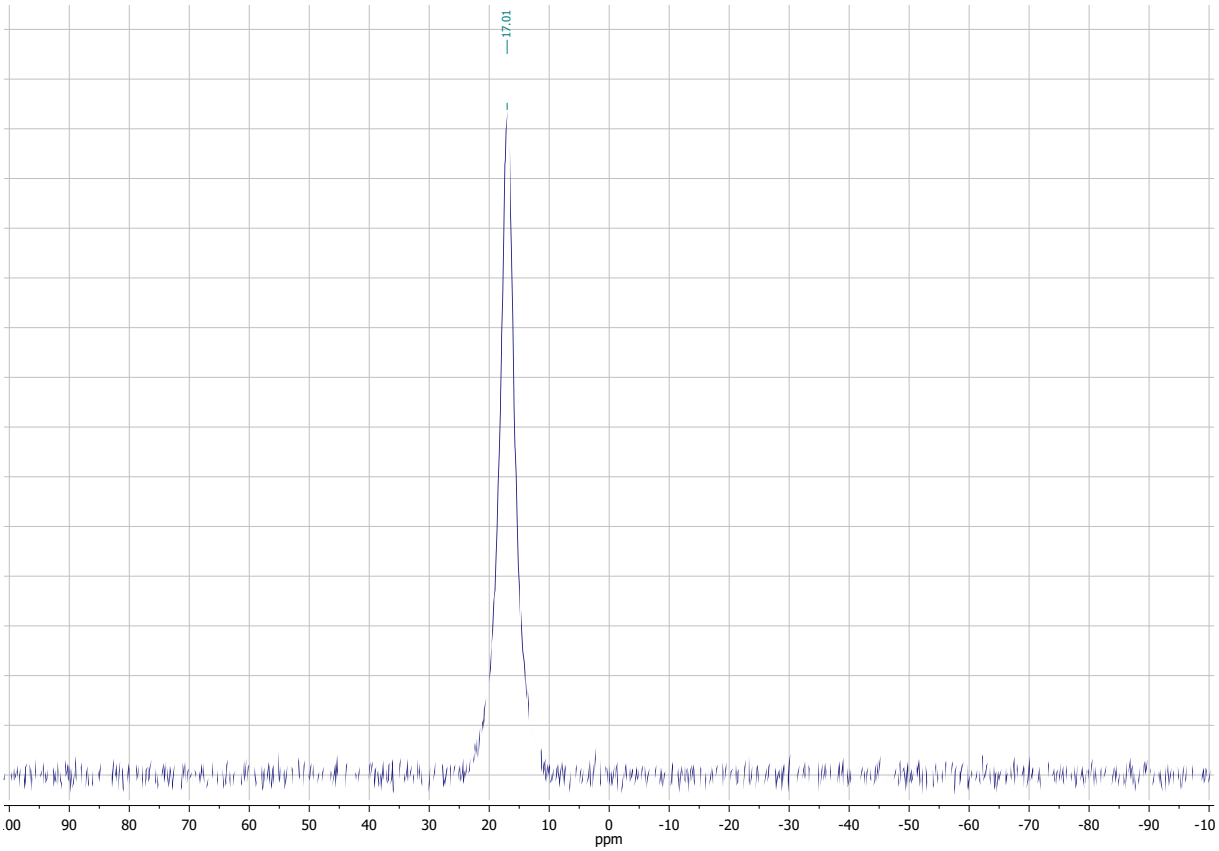

Figure 16 $^{11}B\{^{1}H\}$ NMR (139 MHz, CD_2Cl_2, 27 °C) spectrum of **2**

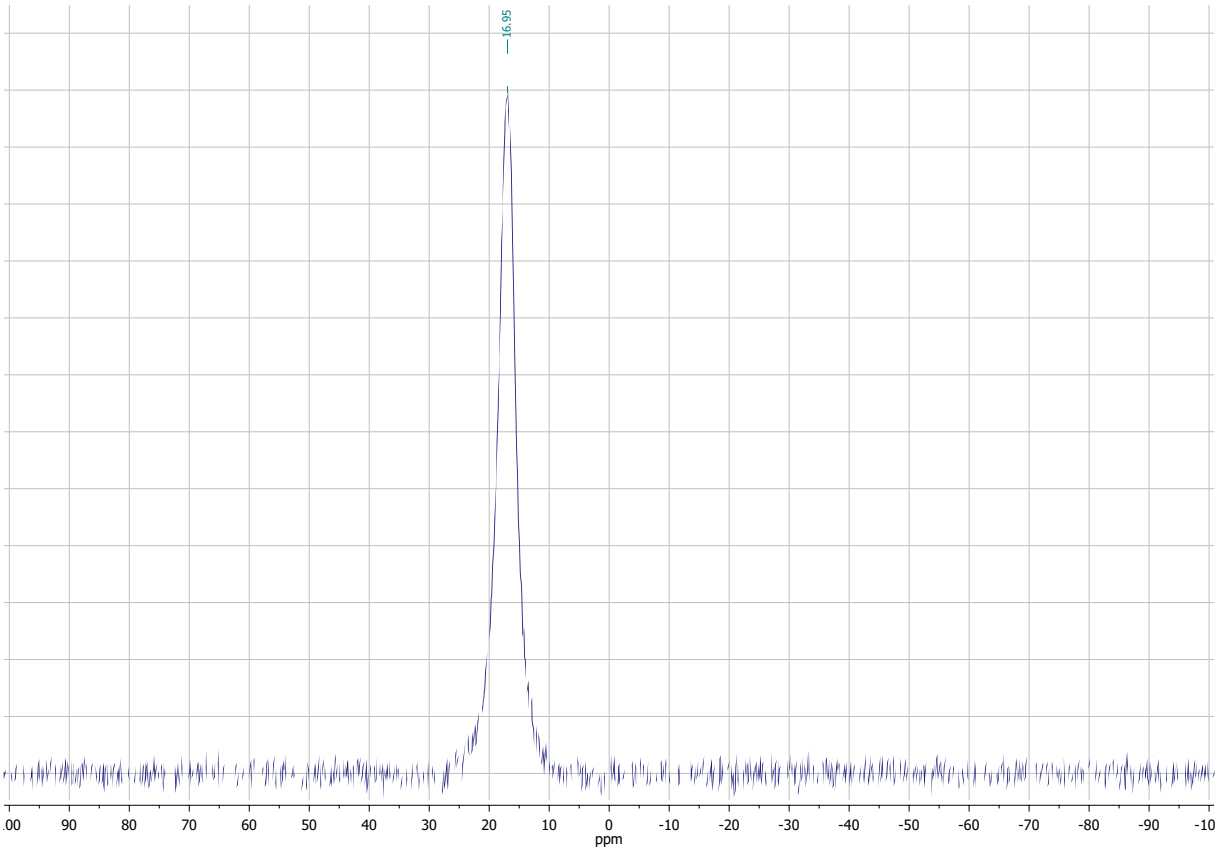

Figure 17 ^{11}B NMR (139 MHz, CD_2Cl_2, 27 °C) spectrum of **2**

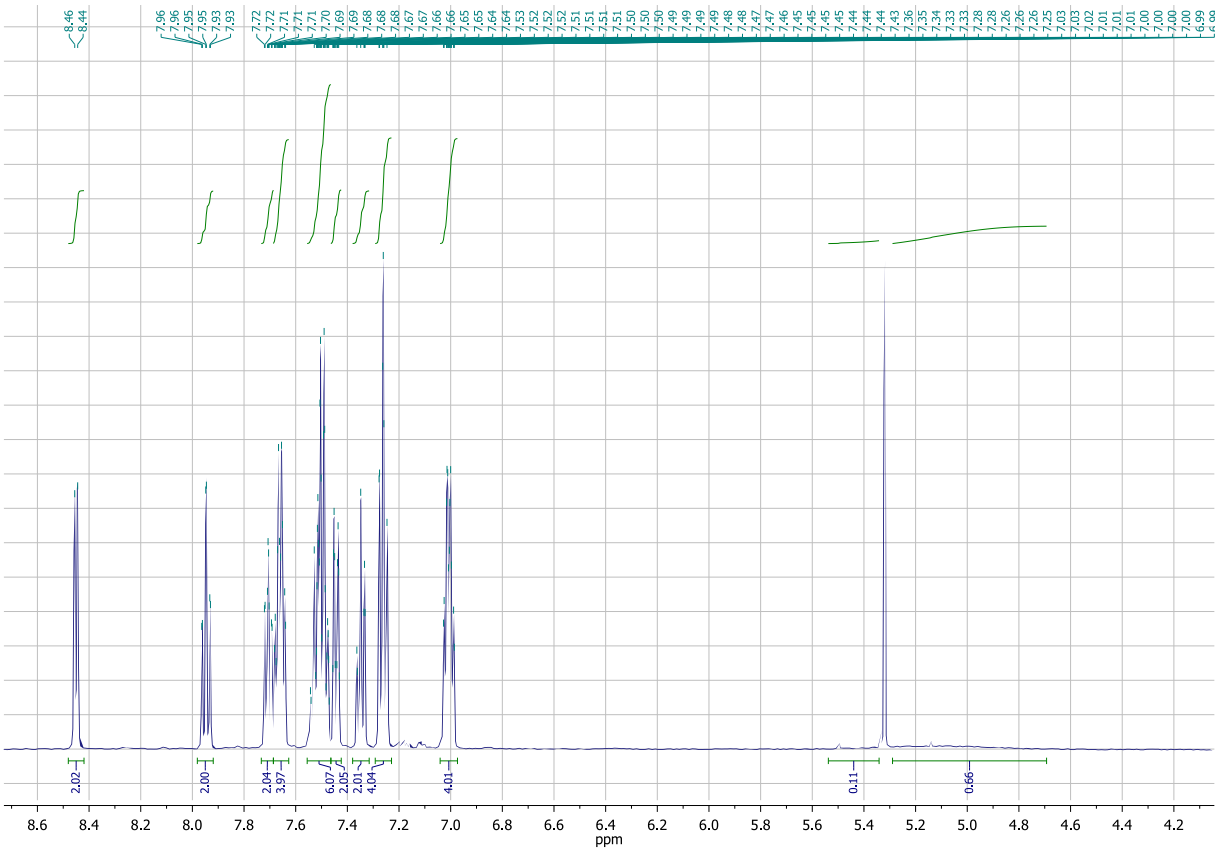

Figure 18 ^{1}H NMR (499.72 MHz, CD_2Cl_2, 27 °C) spectrum of **2**

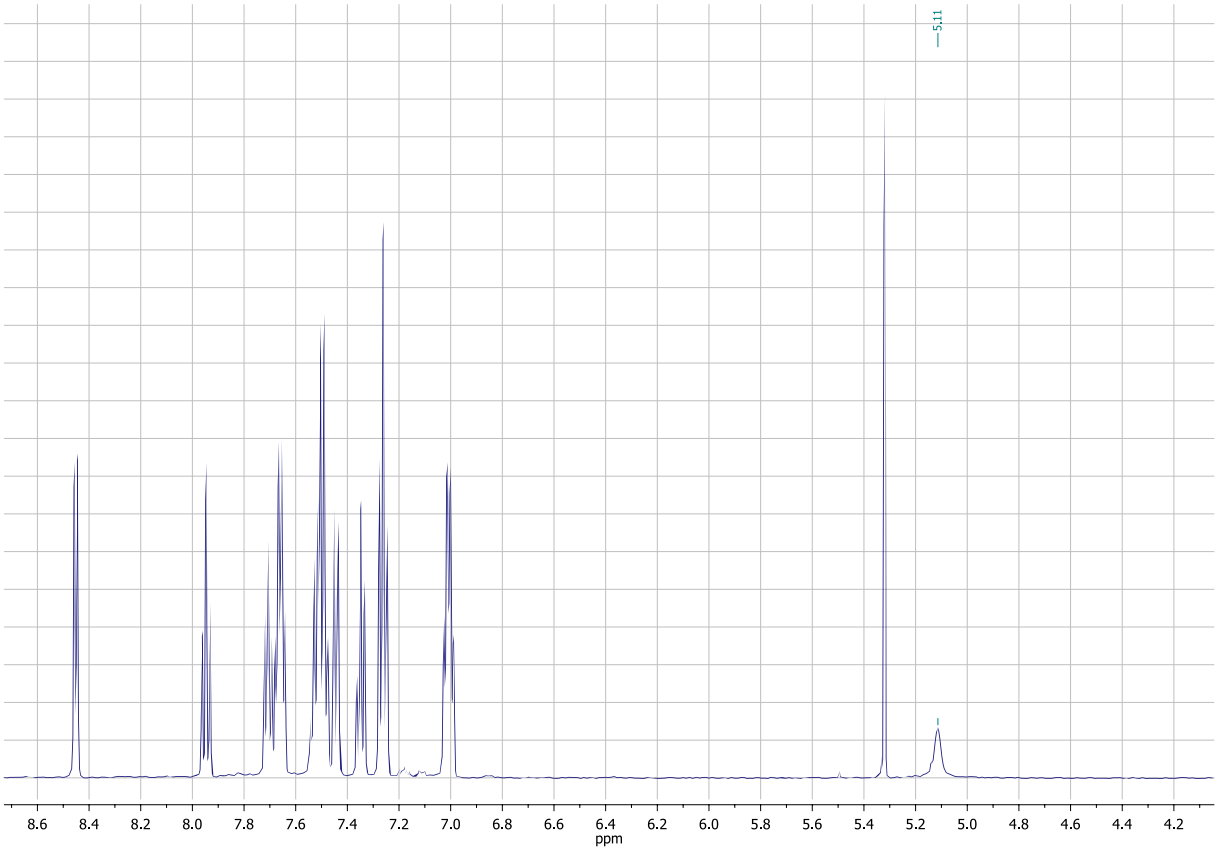

Figure 19 $^{1}H\{^{11}B\}$ NMR (499.72 MHz, CD_2Cl_2, 27 °C) spectrum of **2**

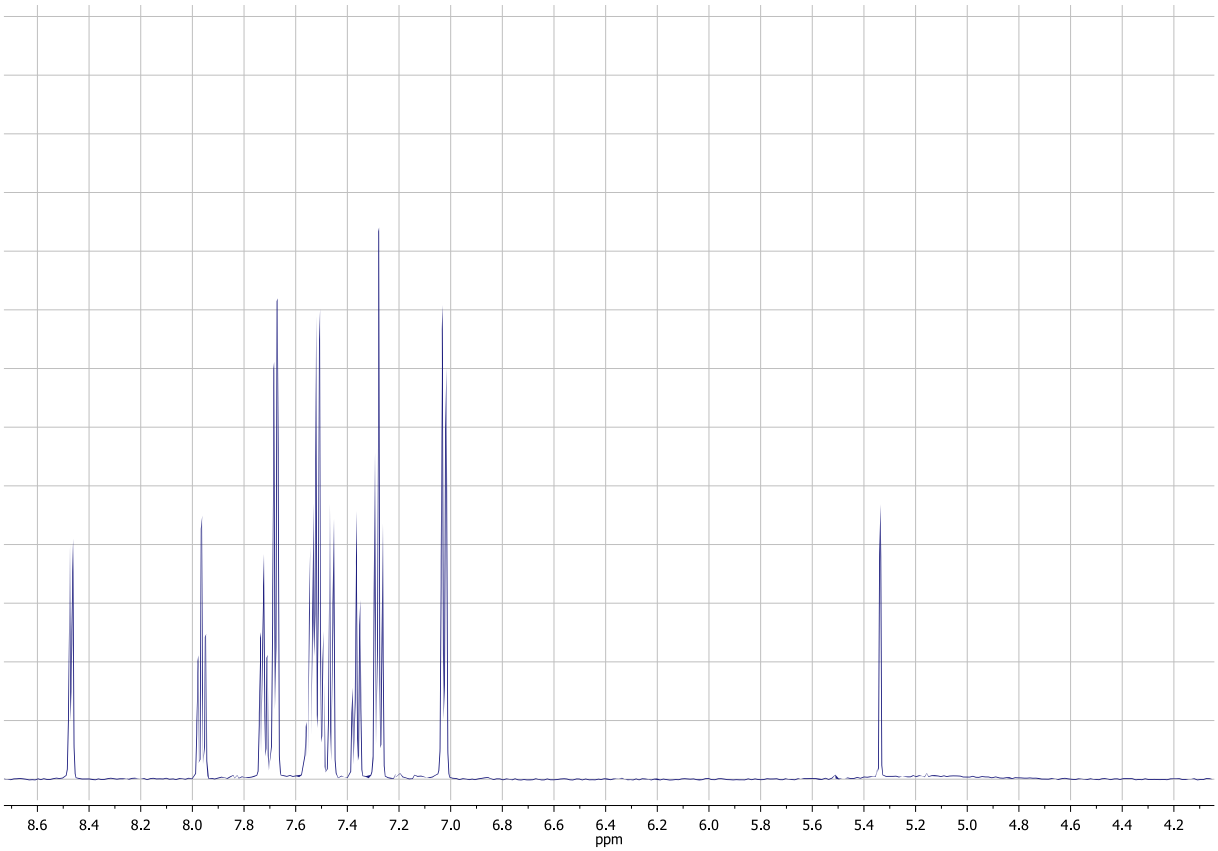

Figure 20 $^{1}H\{^{31}P\}$ NMR (499.72 MHz, CD_2Cl_2, 27 °C) spectrum of **2**

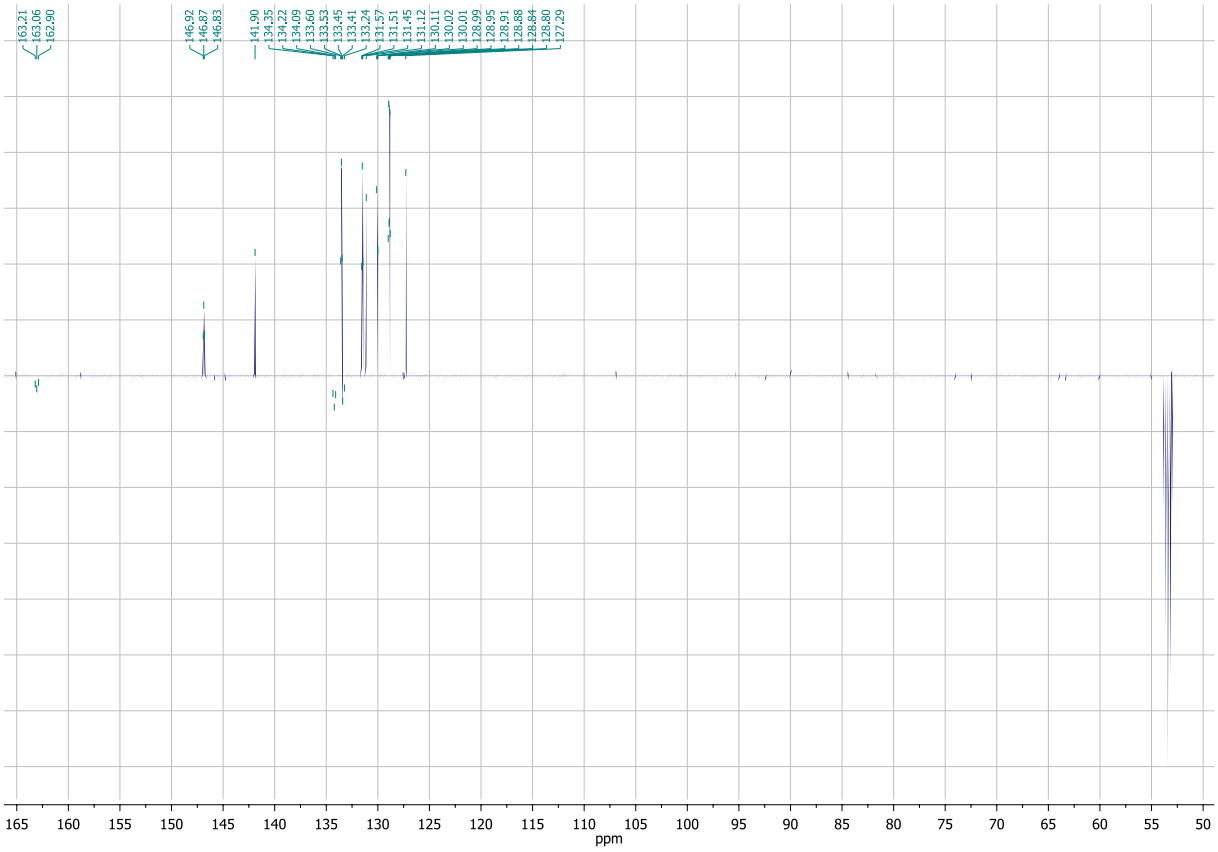

Figure 21 ^{13}C APT NMR (126 MHz, CD_2Cl_2, 27 °C) spectrum of **2**

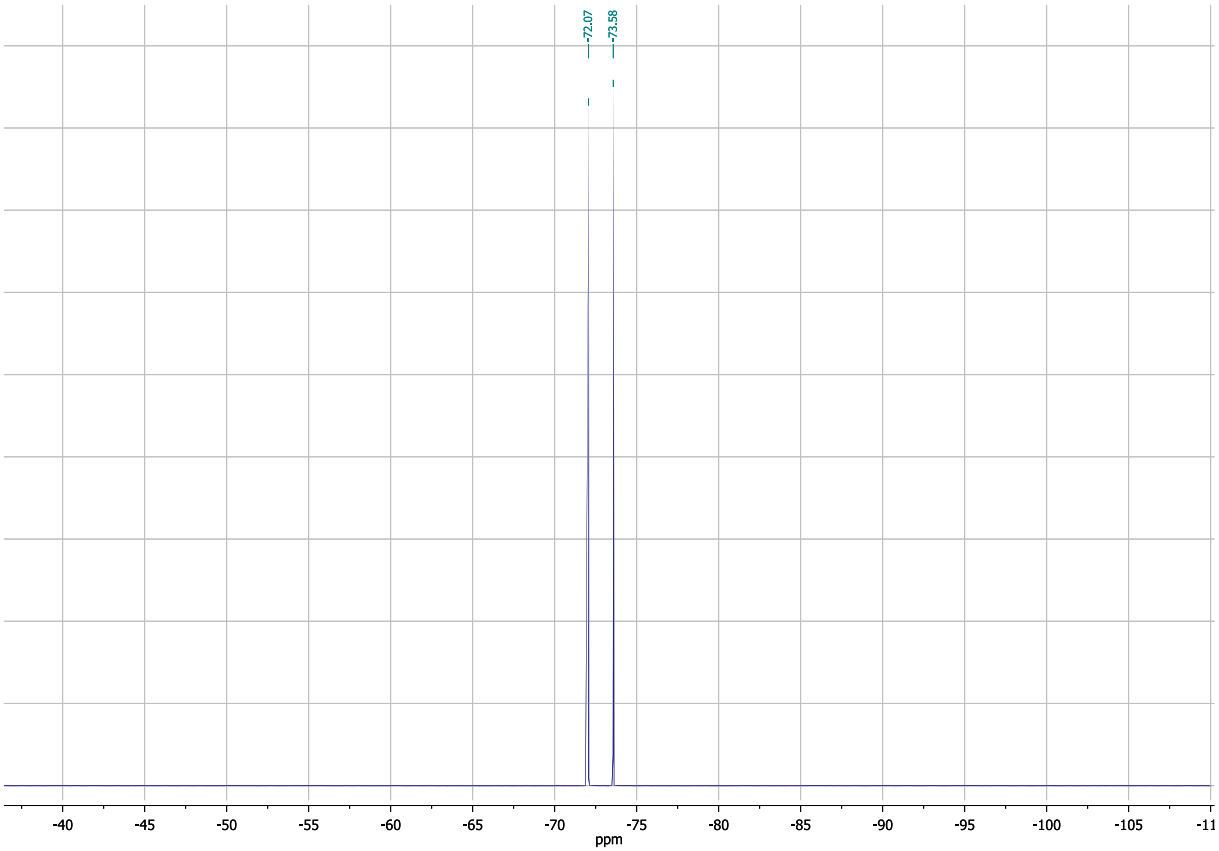

Figure 22 $^{19}F\{^{1}H\}$ NMR (470 MHz, CD_2Cl_2, 27 °C) spectrum of **2**

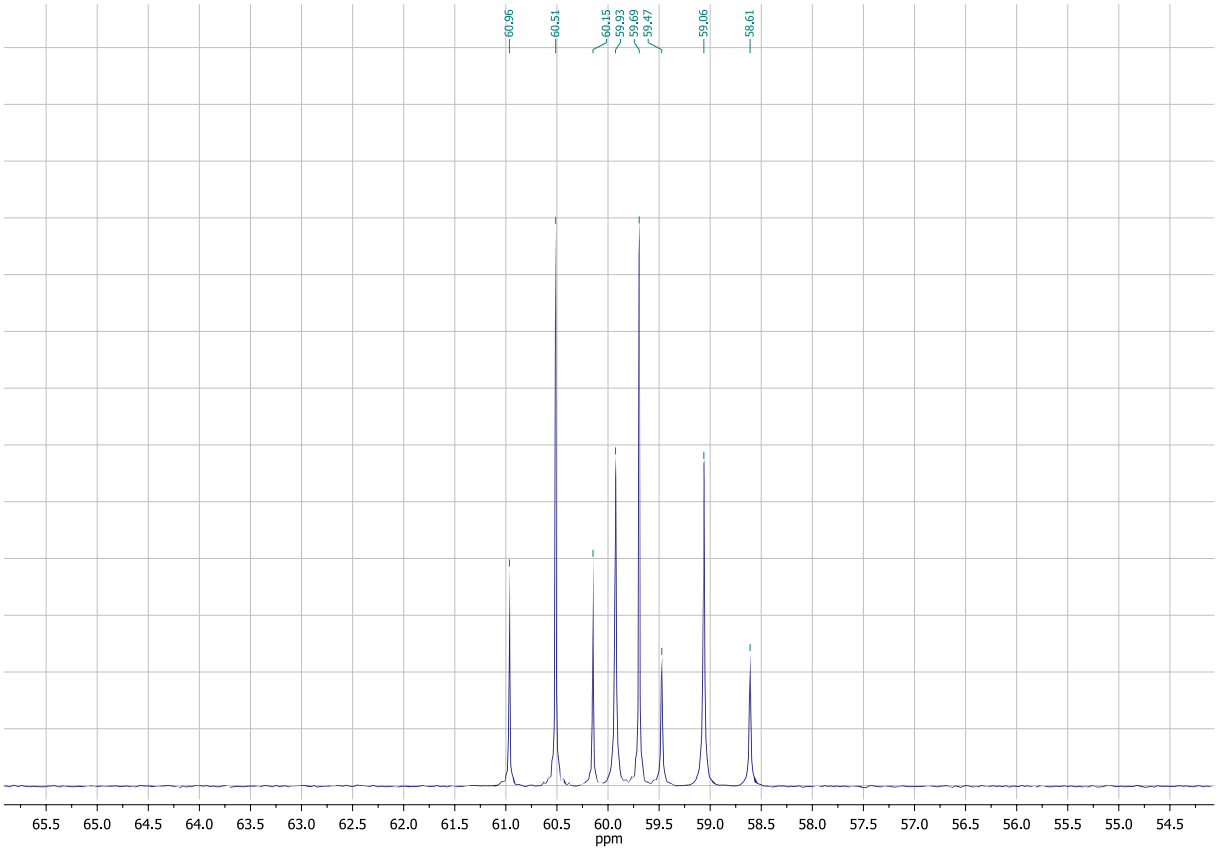

Figure 23 $^{31}P\{^{1}H\}$ NMR (202 MHz, CD_2Cl_2) spectrum of **3**

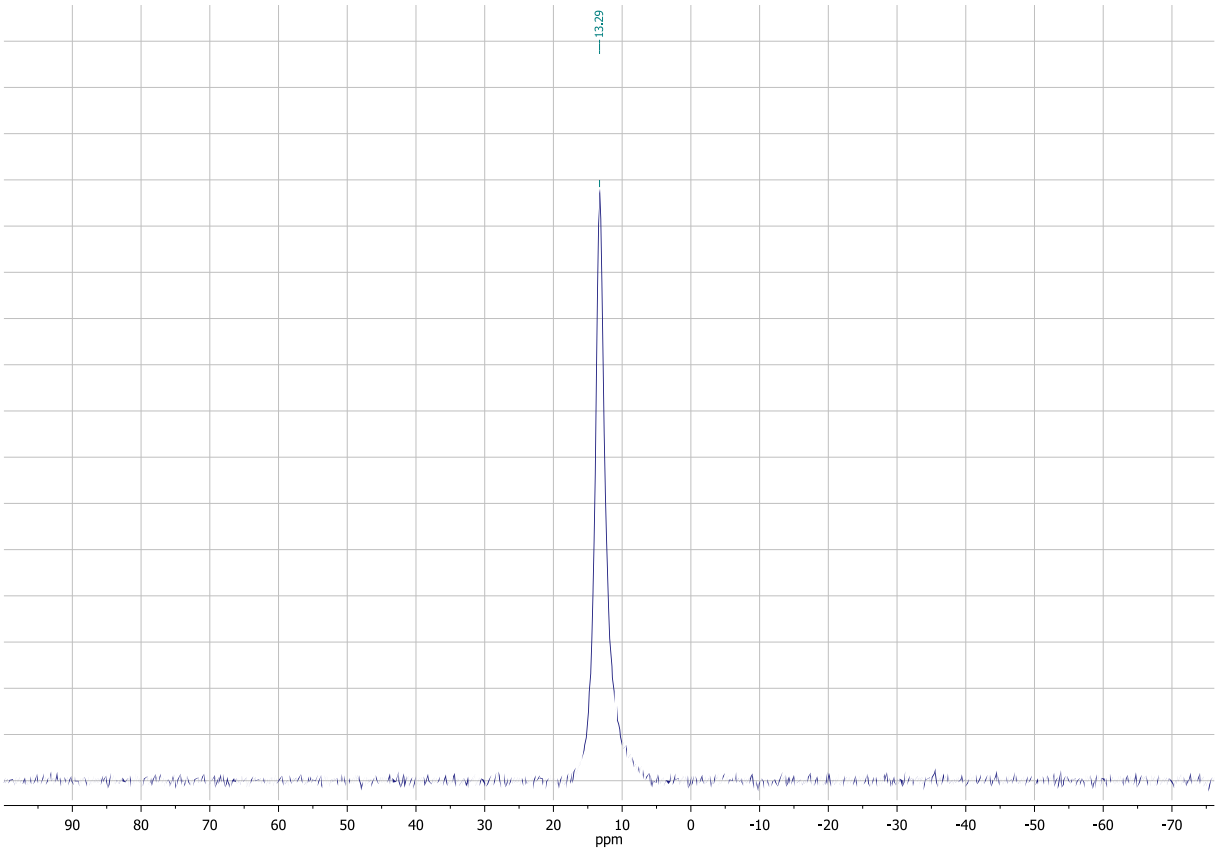

Figure 24 $^{11}B\{^{1}H\}$ NMR (160 MHz, CD_2Cl_2, 27 °C) spectrum of **3**

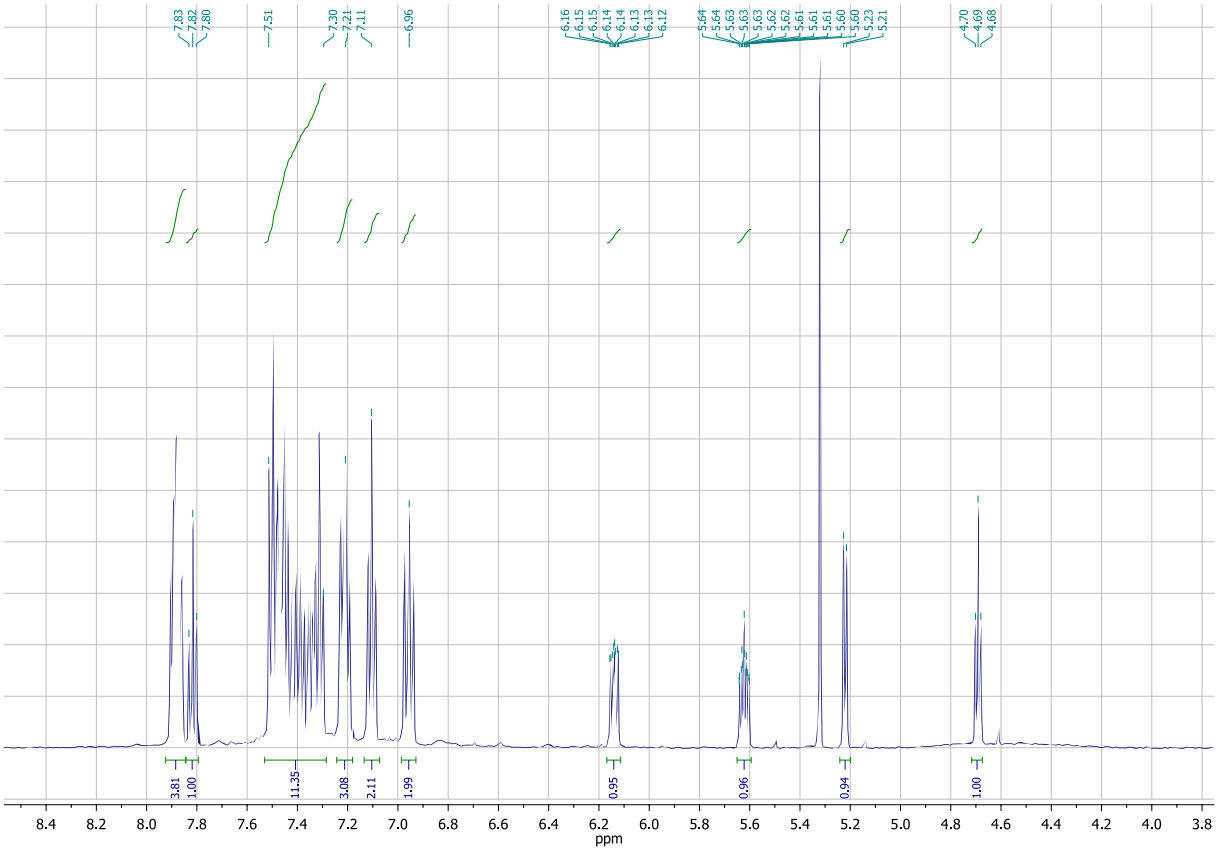

Figure 25 ^{1}H NMR (499.72 MHz, CD_2Cl_2, 27 °C) spectrum of **3**

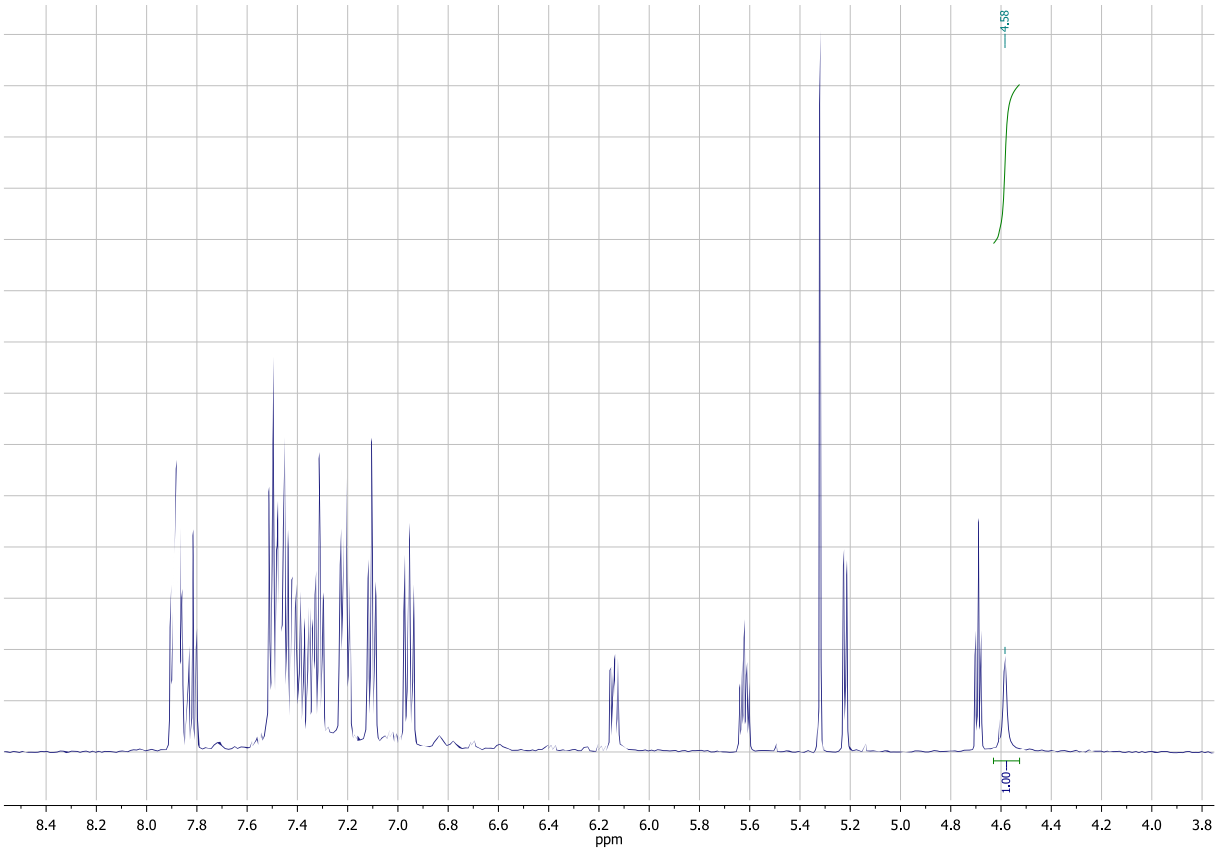

Figure 26 $^{1}H\{^{11}B\}$ NMR (499.72 MHz, CD_2Cl_2, 27 °C) spectrum of **3**

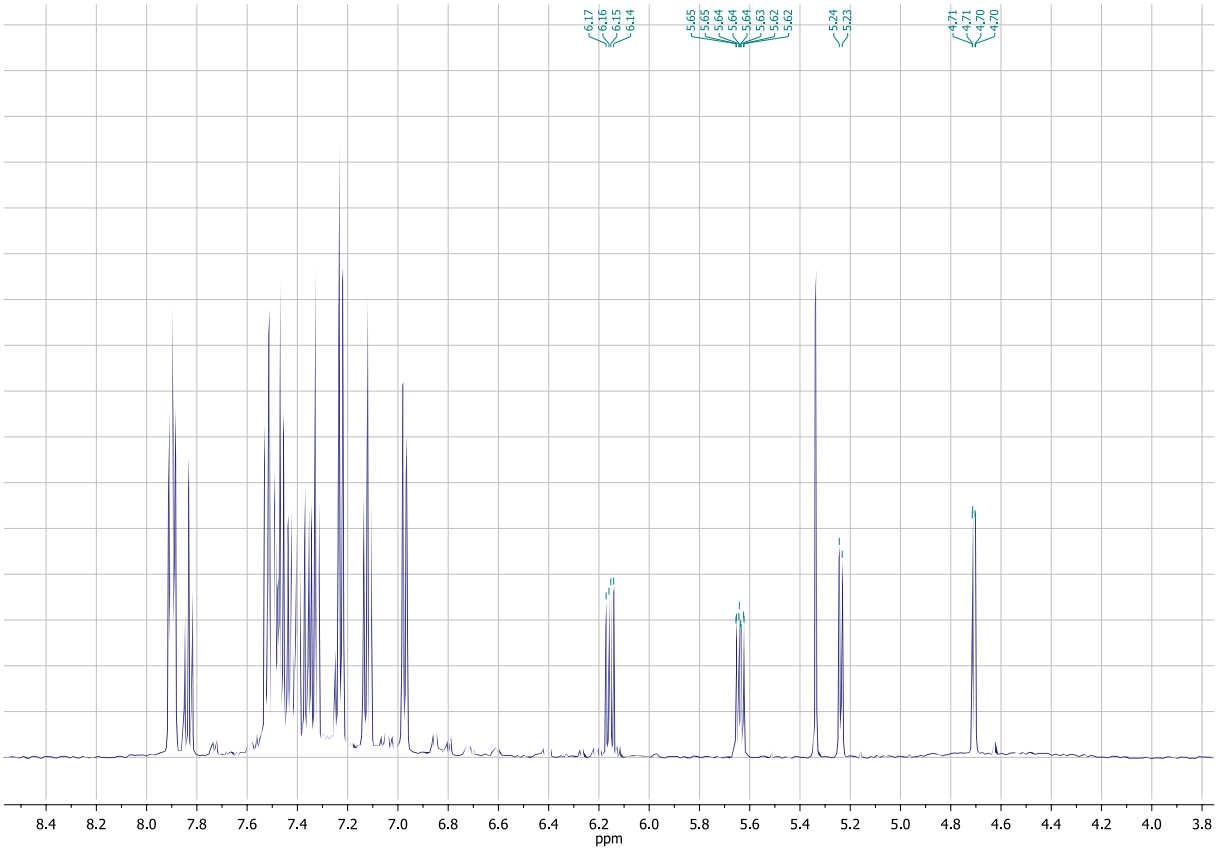

Figure 27 $^{1}H\{^{31}P\}$ NMR (499.72 MHz, CD_2Cl_2, 27 °C) spectrum of **3**

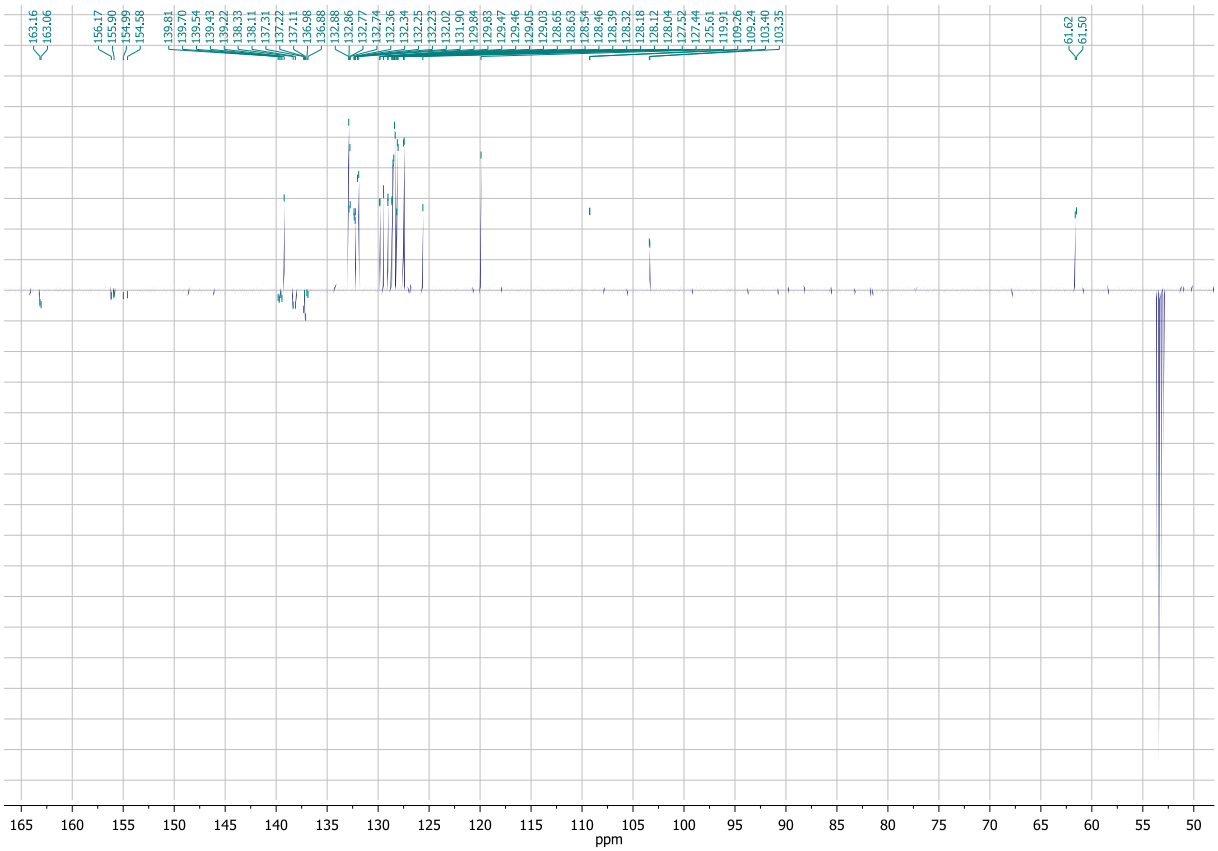

Figure 28 ^{13}C APT NMR (126 MHz, CD_2Cl_2, 27 °C) spectrum of **3**

FT-IR Spectra

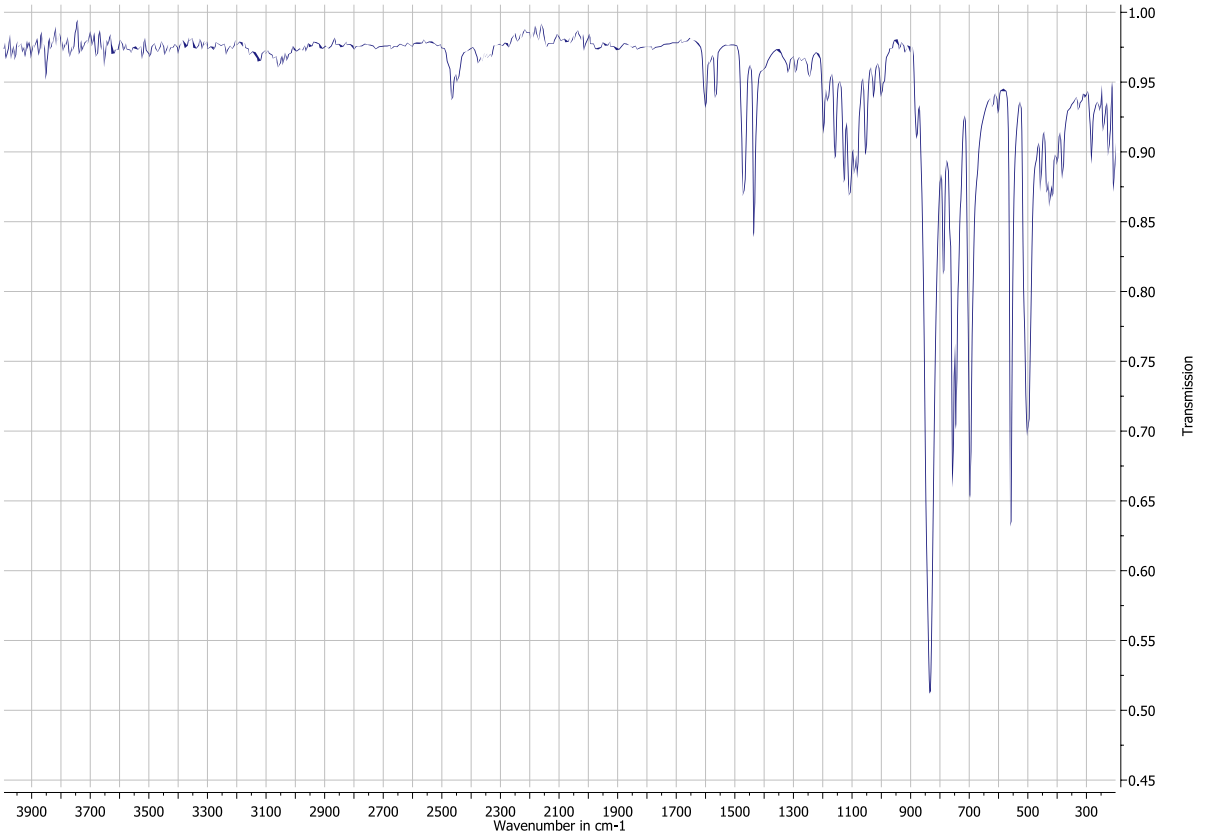

Figure 29 FT-IR spectrum of **1**

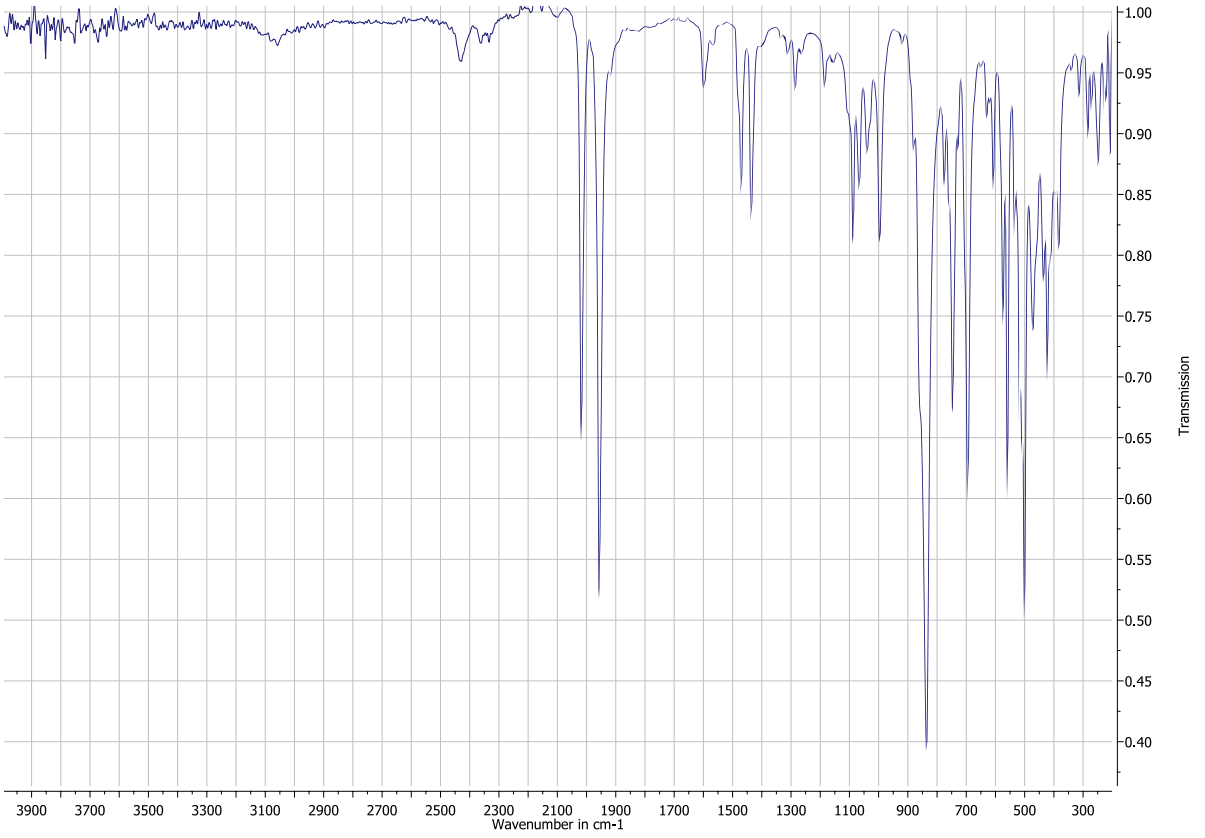

Figure 30 FT-IR spectrum of **2**

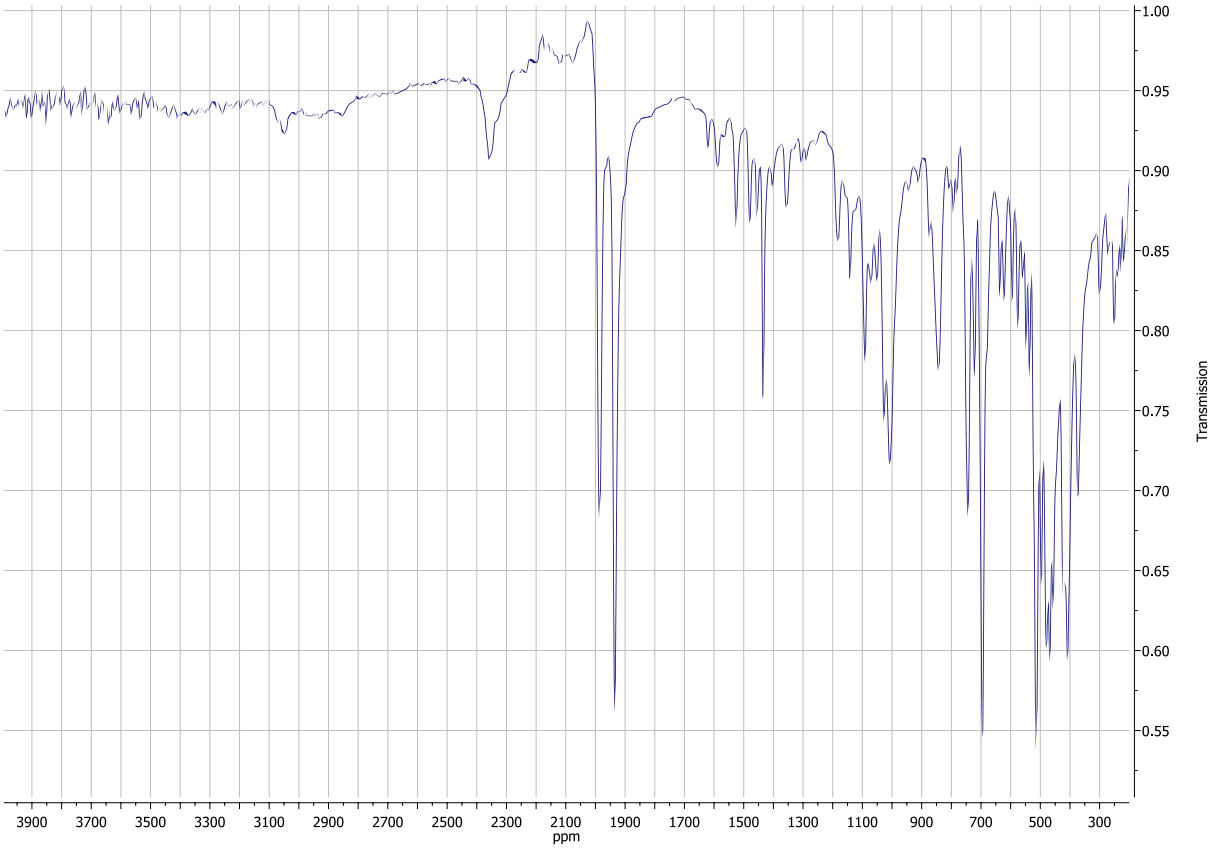

Figure 31 FT-IR spectrum of **3**

MS Spectra

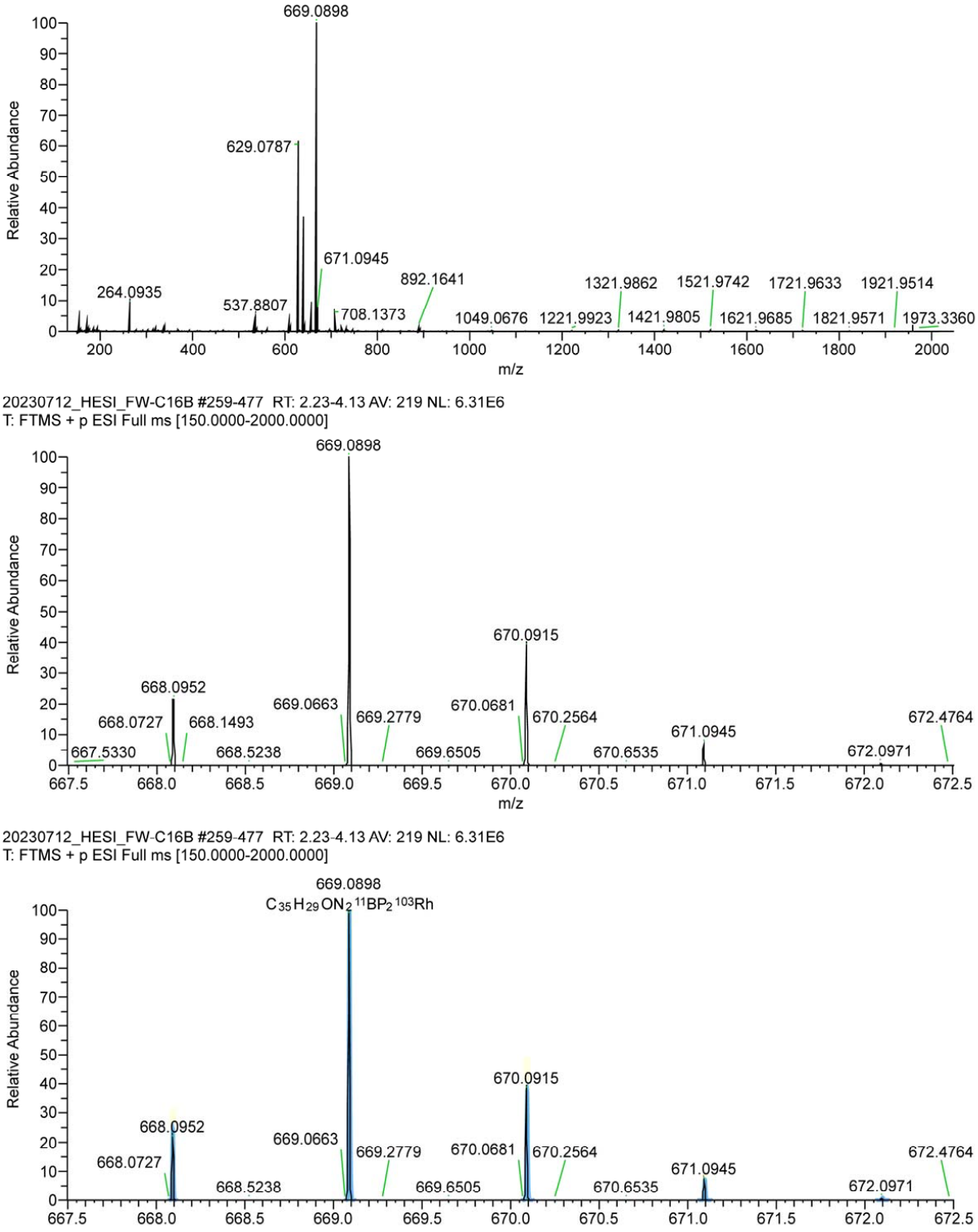

Figure 32 HR-MS spectrum (positive Mode, HESI) of **2**, full spectrum (top), measured isotope pattern (middle) and calculated isotope pattern (bottom)

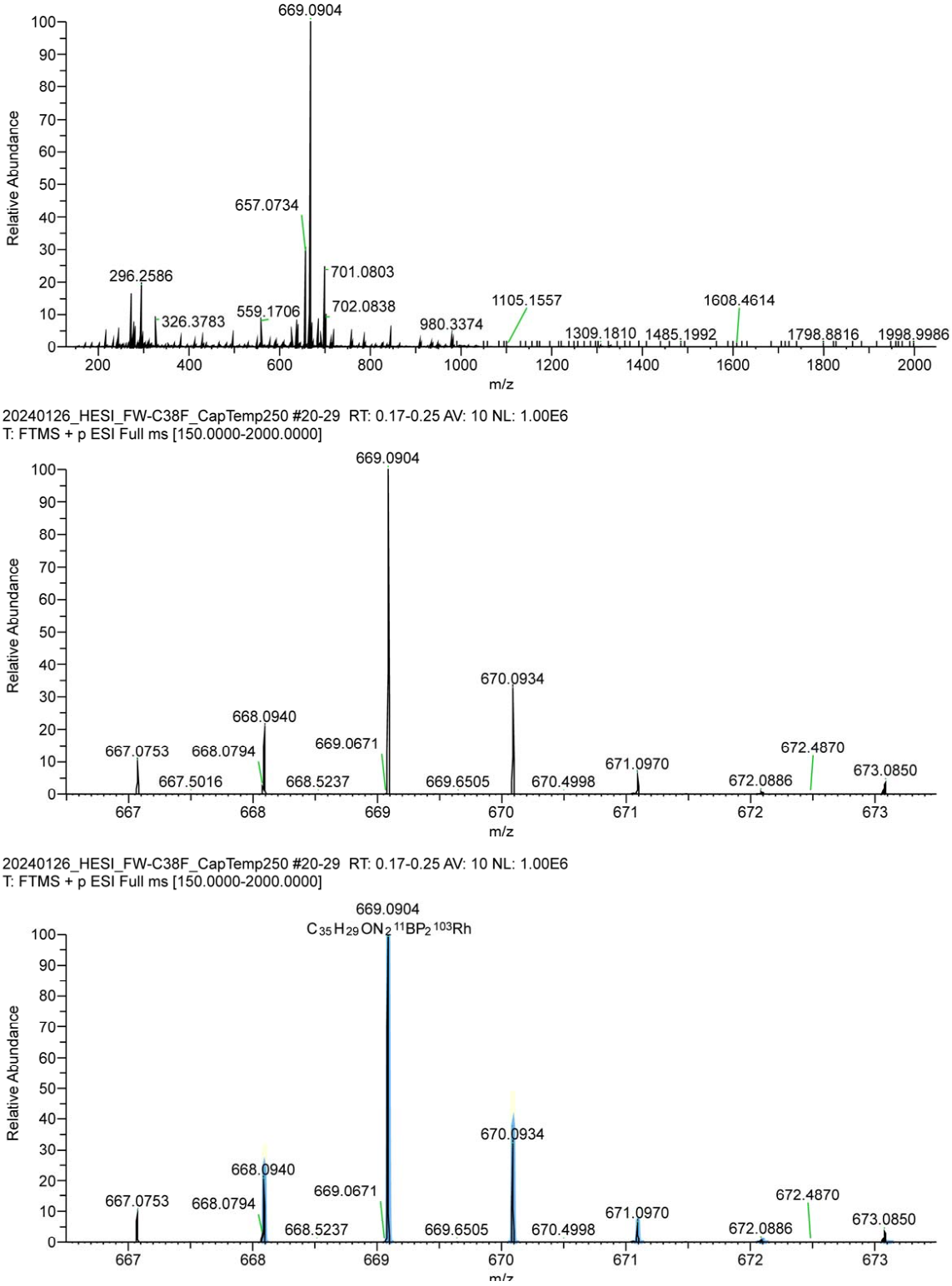

Figure 33 HR-MS spectrum (positive Mode, HESI) of **3**, full spectrum (top), measured isotope pattern (middle) and calculated isotope pattern (bottom)

X-Ray Crystallography

The single crystal X-ray diffraction data for the structural analysis were collected using graphite-monochromated Mo-Kα-radiation (λMoKα= 0.71073) on an imaging plate system STOE IPDS2T and IPDS2. The structures were solved with implemented SHELXT into the Olex2 software package version 1.5 by intrinsic phasing method and refined against F2 by full-matrix-least- square techniques using SHELXL.[1–4] Crystallographic data for **1**, **2** and **3** was deposited at Cambridge Crystallographic Data Centre (CCDC 2385381 - 2385383) and can be obtained free of charge via www.ccdc.cam.ac.uk/. Selected Crystallographic data is summarized in Table *1*.

Table 1 Crystallographic data of Compounds **1**, **2** and **3**.

Compound	**1**	**2**	**3**·$^1/_2$THF
Formula	$C_{34}H_{30}BF_6N_2P_3$	$C_{36}H_{29}BF_6N_2O_2P_3Rh$	$C_{36}H_{28}BN_2O_2P_2Rh\cdot{}^1/_2C_4H_8O$
M / g·mol^{-1}	684.35	842.26	696.28
T/K	170	170	170
Crystal System	Triclinic	Monoclinic	Monoclinic
Space Group	$P\bar{1}$	$P2_1/n$	$C2/c$
a / Å	10.456(2)	10.859(2)	30.217(6)
b / Å	10.633(2)	9.874(2)	14.648(3)
c / Å	16.833(3)	33.638(7)	17.297(4)
α / °	83.37(3)	90	90
β / °	77.74(3)	95.65(3)	118.60(3)
γ / °	62.19(3)	90	90
V / Å^3	1617.3(7)	3589.2(13)	6722(3)
Z	2	4	8
$\rho_{calc.}$ / g·cm^{-3}	1.405	1.559	1.376
μ / mm^{-1}	0.247	0.677	0.637
F(000)	704	1696	2832
Θ_{min} / °	2.166	1.217	1.535
Θ_{max} / °	25.999	25.686	25.993
Measured Refl.	14051	21091	26240
Independent Refl.	6334 (R_{Int} = 0.0403)	6686 ($_{RInt}$ = 0.0717)	6598 ($_{RInt}$ = 0.0276)
Ind. Refl. (I>2σ(I))	5488	5693	5891
Parameters / Restraints	423 / 0	464 / 0	401 / 0
R_1	0.0366	0.0513	0.0217
R_1 (all data)	0.0434	0.0596	0.0252
wR_2	0.0969	0.1375	0.0555
wR_2 (all data)	0.1010	0.1468	0.0572
GooF	1.042	1.073	1.035
Max. peak + hole / e·Å^{-3}	0.345 / -0.306	2.532 / -0.792	0.390 / -0.251
CCDC	2385381	2385382	2385383

Computational Details

Educts, intermediates, transition states and products of the deprotonation were optimized by the density functional theory (DFT)[5] with Grimme's B97D3 functional[6,7] and the def2svp basis set[8,9] in the gas phase using Gaussian16.[10] Frequency analysis calculations of optimized structures were performed at the same level of theory (B97D3/def2svp) to characterize the structures to be minima (no imaginary frequency) or transition states (one imaginary frequency). Based on the B97D3/def2svp optimized geometries, the energy results were further refined by calculating the single point energy at the B97D3/def2tzvp level of theory. The bulky solvation effect of THF was simulated by SMD[11] continuum solvent mode at the B97D3/def2tzvp level of theory. Intrinsic reaction coordinate (IRC) calculations were performed to confirm the connection between two correct minima for a transition state. For bonding analysis of complexes **2**-**4** geometry optimisations and frequency calculations were calculated on B97D3/def2tzvpp level of theory. Laplacian contour line plots (Figure 4) were created with the program Multiwfn.[12] xyz-coordinates are available as separate files.

In preliminary investigations, the proton affinities (PA's) were calculated on def2-SVP/B97D3 level of theory as the difference in Gibbs energy (E) between a protonated complex and it's deprotonated counterpart:

$$PA = E(\text{complex}) - E(\text{complexH}^+)$$

Not included in the calculations were counter ions and implicit or explicit solvation effects. In Fig. 34 the calculated Pas of different deprotonated species are summarized.

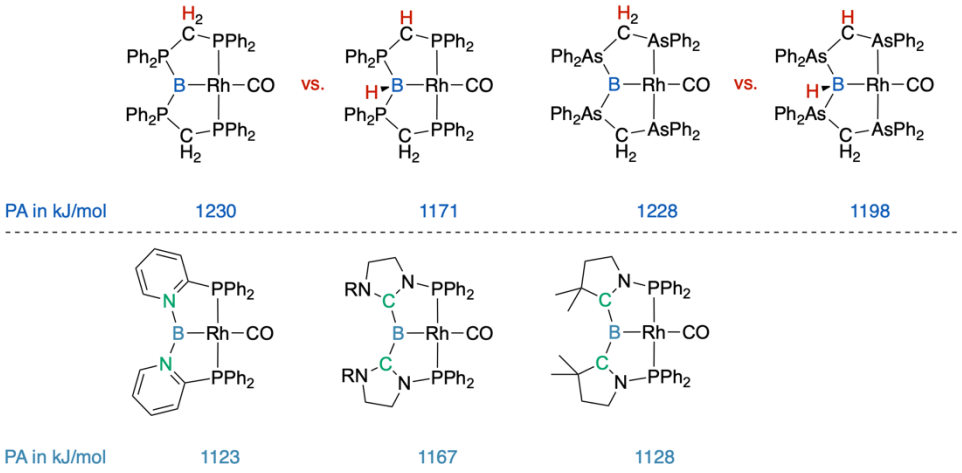

Figure 34 Calculated proton affinities if different deprotonated species.

References

1 O. V. Dolomanov, L. J. Bourhis, R. J. Gildea, J. A. K. Howard and H. Puschmann, *J Appl Crystallogr*, 2009, **42**, 339–341.
2 L. J. Bourhis, O. V. Dolomanov, R. J. Gildea, J. A. K. Howard and H. Puschmann, *Acta Crystallogr A Found Adv*, 2015, **71**, 59–75.
3 G. M. Sheldrick, *Acta Crystallogr A Found Crystallogr*, 2008, **64**, 112–122.
4 G. M. Sheldrick, *Acta Crystallogr A Found Adv*, 2015, **71**, 3–8.
5 P. Hohenberg and W. Kohn, *Phys. Rev.*, 1964, **136**, B864–B871.
6 S. Grimme, *J Comput Chem*, 2006, **27**, 1787–1799.
7 S. Grimme, S. Ehrlich and L. Goerigk, *J Comput Chem*, 2011, **32**, 1456–1465.
8 F. Weigend, *Phys. Chem. Chem. Phys.*, 2006, **8**, 1057.
9 F. Weigend and R. Ahlrichs, *Phys. Chem. Chem. Phys.*, 2005, **7**, 3297.
10 Gaussian 16, Revision C.01, M. J. Frisch, G. W. Trucks, H. B. Schlegel, G. E. Scuseria, M. A. Robb, J. R. Cheeseman, G. Scalmani, V. Barone, G. A. Petersson, H. Nakatsuji, X. Li, M. Caricato, A. V. Marenich, J. Bloino, B. G. Janesko, R. Gomperts, B. Mennucci, H. P. Hratchian, J. V. Ortiz, A. F. Izmaylov, J. L. Sonnenberg, D. Williams-Young, F. Ding, F. Lipparini, F. Egidi, J. Goings, B. Peng, A. Petrone, T. Henderson, D. Ranasinghe, V. G. Zakrzewski, J. Gao, N. Rega, G. Zheng, W. Liang, M. Hada, M. Ehara, K. Toyota, R. Fukuda, J. Hasegawa, M. Ishida, T. Nakajima, Y. Honda, O. Kitao, H. Nakai, T. Vreven, K. Throssell, J. A. Montgomery, Jr., J. E. Peralta, F. Ogliaro, M. J. Bearpark, J. J. Heyd, E. N. Brothers, K. N. Kudin, V. N. Staroverov, T. A. Keith, R. Kobayashi, J. Normand, K. Raghavachari, A. P. Rendell, J. C. Burant, S. S. Iyengar, J. Tomasi, M. Cossi, J. M. Millam, M. Klene, C. Adamo, R. Cammi, J. W. Ochterski, R. L. Martin, K. Morokuma, O. Farkas, J. B. Foresman, and D. J. Fox, Gaussian, Inc., Wallingford CT, 2016.
11 A. V. Marenich, C. J. Cramer and D. G. Truhlar, *J. Phys. Chem. B*, 2009, **113**, 6378–6396.
12 T. Lu and F. Chen, *J Comput Chem*, 2012, **33**, 580–592.